NUREG/CR-1130

Two-Phase Flow Phenomena in Nuclear Reactor Technology

Quarterly Progress Report
December 1978 - February 1979

Prepared by R. T. Lahey, Jr.

Rensselaer Polytechnic Institute

Prepared for
U. S. Nuclear Regulatory
Commission

Available from

GPO Sales Program
Division of Technical Information and Document Control
U. S. Nuclear Regulatory Commission
Washington, D. C. 20555

and

National Technical Information Service
Springfield, Virginia 22161

NUREG/CR-1130
R2, R4

Two-Phase Flow Phenomena in Nuclear Reactor Technology

Quarterly Progress Report
December 1978 - February 1979

Manuscript Completed: April 1979
Date Published: November 1979

Prepared by
R. T. Lahey, Jr.

Department of Nuclear Engineering
Rensselaer Polytechnic Institute
Troy, NY 12181

Prepared for
Division of Reactor Safety Research
Office of Nuclear Regulatory Research
U.S. Nuclear Regulatory Commission
Washington, D.C. 20555
NRC FIN No. B5873

ABSTRACT

This Quarterly Progress Report contains a description of the work done in three areas of technology. The significant results are:

I. Two-Phase Flow Instrumentation Development - The recent PNA tagging data is presented. In addition, a detailed error analysis is presented for the side-scatter gamma ray system under development.

II. Phase Distribution and Separation Phenomena - An analytical model for phase separation in Wyes and Tees is presented. In addition, an analytical model for subchannel void-drift is developed.

III. BWR Parallel Channel Effects - The status of the experimental PCE loop and the supporting analysis is presented.

INTRODUCTION

TWO-PHASE FLOW PHENOMENA IN NUCLEAR REACTOR TECHNOLOGY

The research program entitled, "Two-Phase Flow Phenomena in Nuclear Reactor Technology", is sponsored by the U.S. Nuclear Regulatory Commission. The basic purpose of this university research program is to develop a more thorough understanding of the two-phase flow phenomena associated with certain hypothetical nuclear reactor accidents.

The program is divided into three major tasks. Task I is concerned with the development of novel, two-phase flow instrumentation with which some basic two-phase flow parameters can be measured (e.g., void fraction, phase velocity, etc.). This instrumentation is intended for high pressure steam-water application as well as laboratory use.

Task II is concerned with the detailed fluid mechanics of two-phase flow. Specifically, an indepth understanding of two-phase flow multidimensional void distribution mechanisms and phase separation effects will be developed. The basic questions to be answered in this task are:

- Why do the phases distribute the way they do?
- What happens to a two-phase flow when it undergoes axial and/or lateral acceleration?

Task III is intended to address a current safety question concerning the performance of the BWR emergency core cooling (ECC) system. Particular emphasis will be placed on parallel channel effects (PCE) during ECCS operation.

In all three tasks, considerable analytical and experimental work was accomplished during the Eleventh Quarter. The RPI personnel who worked on each task during the report period are tabulated in the following table.

TASK GROUPS

TASK I: TWO-PHASE FLOW INSTRUMENTATION

Senior Investigators:

G. Krycuk
R.T. Lahey, Jr.
R.R. Gay
H.E. Breed
S. Moreira

Graduate Students:

M. Vince
M. Perez-Griffo
N. Saba

TASK II: PHASE SEPARATION & DISTRIBUTION PHENOMENA

Senior Investigators:

D.A. Drew
R.T. Lahey, Jr.
J.E. Flaherty
J.P. Tully

Graduate Students:

L. Cheng
S. Sim
M. Barasch
K. Ohkawa

undergraduate Students:

R. Sterner
J. McKenzie

TASK III: BWR ECC PARALLEL CHANNEL EFFECTS

Senior Investigators:

R.T. Lahey, Jr.
J.P. Tully
J.E. Flaherty

Graduate Students:

W. Conlon
D. Shum
M. Fakory

TABLE OF CONTENTS

LIST OF FIGURES

TASK I

TWO-PHASE FLOW INSTRUMENTATION DEVELOPMENT

This task has as its objective the development of accurate and reliable instrumentation for the measurement of the single and two-phase flow characteristics under a variety of steady-state and transient conditions. Such instrumentation is necessary for the understanding of the results of reactor safety experiments on current generation light water reactors (LWR), such as Semi-Scale, LOFT and BWR-BDHT. To this end a broad program is being conducted for the development of both in-core and out-of-core techniques for the measurement of important multiphase flow parameters such as void fraction, phasic velocity, slip ratio and flow regime.

I.1 PNA Tagging Results

In our previous PNA single-phase flow measurements [1], we observed that in fitting the experimental (time) profiles of the irradiated water with the theory of G.I. Taylor [2], that this theory did reasonably well in predicting the over-all profile but departed from the data near the trailing edge of each pulse. We interpreted this in terms of the effect the laminar sublayer causing prolonged holdup of the N^{16}.

In the two-phase flow series of PNA measurements [3],we found that for very small air flow rates, the air bubbles travelled mostly around the pipe walls (an observation consistent with Serizawa's data [4]) and the resultant time profile of the irradiated pulse fits the Taylor theory quite well. This interesting feature is shown in Figure I.1. Here a single-phase flow time profile is compared to a two-phase flow condition with very small air flow ("champagne" flow). In both cases the theory of G.I. Taylor has been fitted to the data by setting the normalization constant equal to the peak counts/second,and by adjusting the single-phase water velocity so the leading edge

LAMINAR BOUNDARY LAYER DISAPPEARANCE

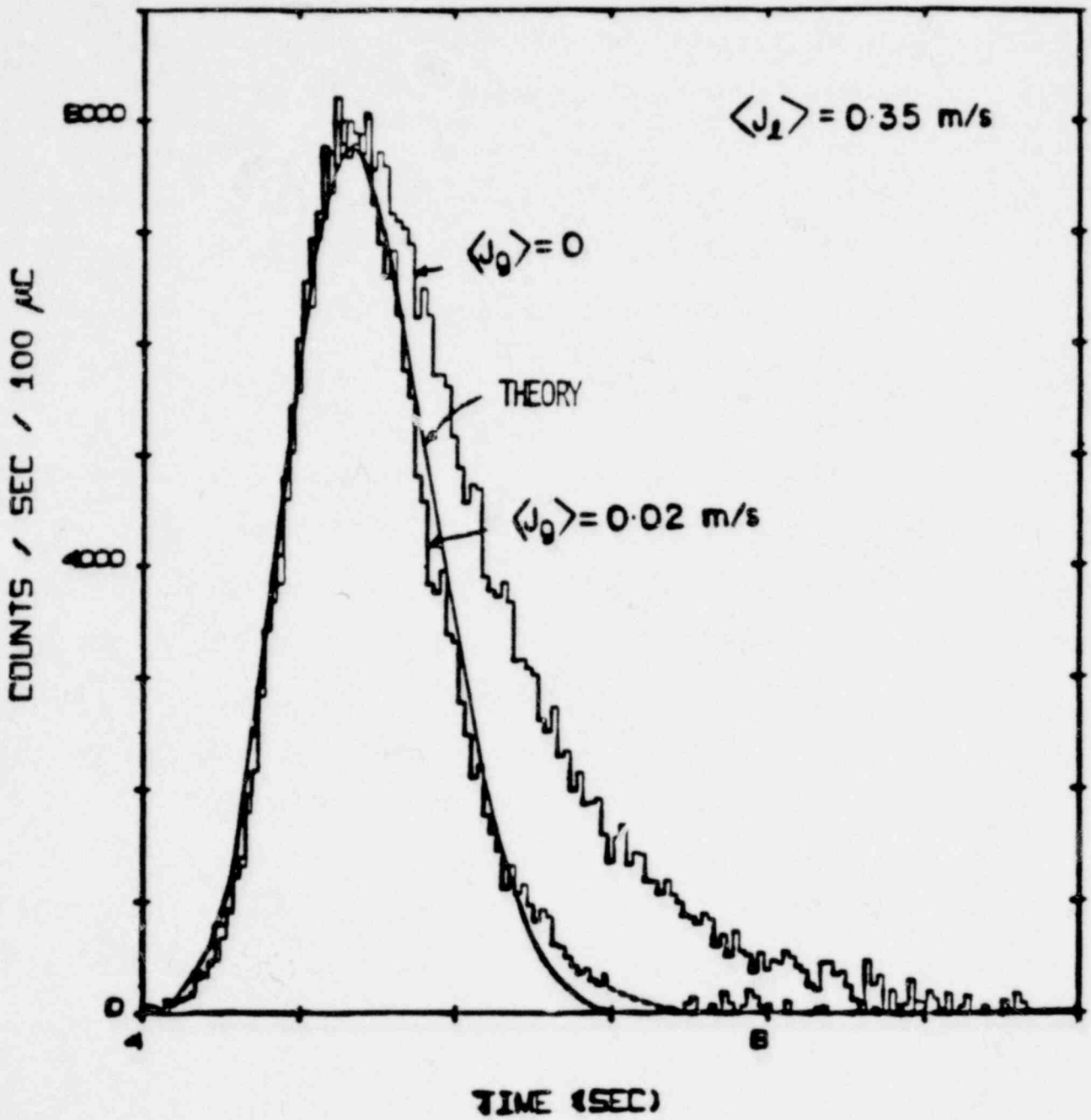

Figure I.1 Comparison between single-phase flow time profile and two-phase flow condition with very small air flow. The continuous line represents the fit by the theory of G. I. Taylor.

of the calculated curve goes through the bulk of the experimental points. It can be seen that the "champagne" flow time profile $\langle j_g \rangle$=0.02m/s(0.06ft/s) fits the theory much better than the single-phase flow time profile.

Based on the above experimental facts, we interpret this result as being due to the small bubbles present in the wall region which apparently disrupt the laminar sublayer near the pipe wall leading to more uniform mixing.

I.2 Side-Scatter Gamma Ray Densitometery

The side-scatter gamma measurement technique being developed at RPI for the measurement of local densities has been described in previous Quarterly Reports [5]. The response of each detector was shown to be:

$$N_1 = C_1 \rho_{sv} \exp(-\beta_1 \rho_{2\phi}) \tag{I.1}$$

$$N_2 = C_2 \rho_{sv} \exp(-\beta_2 \rho_{2\phi}) \tag{I.2}$$

where,

$$\beta_1 \triangleq \left(\frac{\mu}{\rho}\right)^i_{2\phi} X^i_{2\phi} + \left(\frac{\mu}{\rho}\right)^e_{2\phi_1} X^e_{2\phi_1}$$

$$\beta_2 \triangleq \left(\frac{\mu}{\rho}\right)^i_{2\phi} X^i_{2\phi} + \left(\frac{\mu}{\rho}\right)^e_{2\phi_2} X^e_{2\phi_2}$$

and,

$C_1, C_2 \triangleq$ calibration constants

$(\mu/\rho) \triangleq$ mass attenuation coefficient

$X \triangleq$ gamma beam path length

$\rho \triangleq$ density

The subscripts are:

1,2 - refers to detector 1 or detector 2

2φ - denotes two-phase flow in the channel

i - the incoming gamma beam

e - the gamma beam exiting the scattering volume

sv - denotes the scattering volume

Combining equations (I.1) and (I.2) and solving for the local scattering volume density yields:

$$\rho_{sv} = \left[\frac{C_2^{\beta_1} N_1^{\beta_2}}{C_1^{\beta_2} N_2^{\beta_1}} \right]^{\frac{1}{\beta_2 - \beta_1}} \tag{I.3}$$

The above expressions were derived assuming that the densities are time independent, while actual densities will fluctuate with time. In order to determine the effect of this dynamic characteristic of two-phase flow, it is assumed that the scattering volume density varies between a maximum and minimum value of,

$$\rho_{sv_{max}} = \rho_{sv_o} (1 + \varepsilon) \tag{I.4}$$

$$\rho_{sv_{min}} = \rho_{sv_o} (1 - \varepsilon) \tag{I.5}$$

Similarly for the chordal average flow channel density,

$$\rho_{2\phi_{max}} = \rho_{2\phi_o} (1 + \Delta) \tag{I.6}$$

$$\rho_{2\phi_{min}} = \rho_{2\phi_o} (1 - \Delta) \tag{I.7}$$

There are four possible combinations of densities in the scattering volume,and along the two-phase beam path,respectively. These are,

(a). $(\rho_{sv_{max}}, \rho_{2_{\phi max}})$

(b). $(\rho_{sv_{max}}, \rho_{2\phi_{min}})$

(c). $(\rho_{sv_{min}}, \rho_{2\phi_{max}})$

(d) $(\rho_{sv_{min}}, \rho_{2\phi_{min}})$

Letting the parameters a, b, c and d represent the fraction of time in which the flow conditions (a), (b), (c) and (d) occur, the count rate of detector-1 becomes,

$$N_1 = C_1 \left\{ a\rho_{sv_{max}} \exp(-\beta_1\rho_{2\phi_{max}}) + b\rho_{sv_{max}} \exp(-\beta_1\rho_{2\phi_{min}}) \right.$$
$$\left. + c\,\rho_{sv_{min}} \exp(-\beta_1\rho_{2\phi_{max}}) + d\,\rho_{sv_{min}} \exp(-\beta_1\rho_{2\phi_{min}}) \right\} \qquad (I.8)$$

A similar expression holds for N_2. The true time-averaged density in the scattering volume is now,

$$\bar{\rho}_{sv} = (a + b)\,\rho_{sv_{max}} + (c + d)\,\rho_{sv_{min}} \qquad (I.9)$$

If the measured density equals the above expression then the dynamic bias is zero, however, generally,this won't be the case.

Substituting the dynamic expressions for the detector count rates into Equation (I.3) for the general case of a local density measurement in a large pipe, the measured scattering volume density is,

$$\rho_{sv_{meas}} = \left[\frac{C_2^{\beta_1} \left\{ a\rho_{sv_{max}} e^{-\beta_1 \rho_{2\phi_{max}}} + b\rho_{sv_{max}} e^{-\beta_1 \rho_{2\phi_{min}}} \right.}{C_1^{\beta_2} \left\{ a\rho_{sv_{max}} e^{-\beta_2 \rho_{2\phi_{max}}} + b\rho_{sv_{max}} e^{-\beta_2 \rho_{2\phi_{min}}} \right.} \right.$$

$$\left. \left. \frac{+ c\rho_{sv_{min}} e^{-\beta_1 \rho_{2\phi_{max}}} + d\rho_{sv_{min}} e^{-\beta_1 \rho_{2\phi_{min}}} \right\}^{\beta_2}}{+ c\rho_{sv_{min}} e^{-\beta_2 \rho_{2\phi_{max}}} + d\rho_{sv_{min}} e^{-\beta_2 \rho_{2\phi_{min}}} \right\}^{\beta_1}} \right]^{\frac{1}{\beta_2 - \beta_1}}$$

It can be easily shown that the dynamic bias appears only in the exponential terms, i.e. the bias disappears as $(\beta_1 \rho_{2\phi})$ approaches zero. Therefore, the value of ε , which defines the magnitude of the fluctuations of ρ_{sv}, makes no contribution to the dynamic measurement error. It is only the fluctuations in the density of the incoming and exiting gamma beam paths which produce dynamic bias in side-scatter systems.

Figure I.2 illustrates the effect of Δ on the dynamic bias. The relative error in density increases monotonically with Δ. Figure I.3 illustrates the effect of increasing the two-phase path length from the source to the scattering volume; and, hence, β_1 and β_2. As expected the error increases with distance into the flow channel. It can be seen that the potential errors due to dynamic basis can be quite large. Clearly this is an area which needs further investigation if we hope to use this system for the measurement of local void fraction.

ρ_{sv_o} = 500 Kg/m^3

$\rho_{2\phi_o}$ = 500 Kg/m^3

$X^i_{2\phi}$ = .04 m

a = b = c = d = 0.25

ε = 1.0

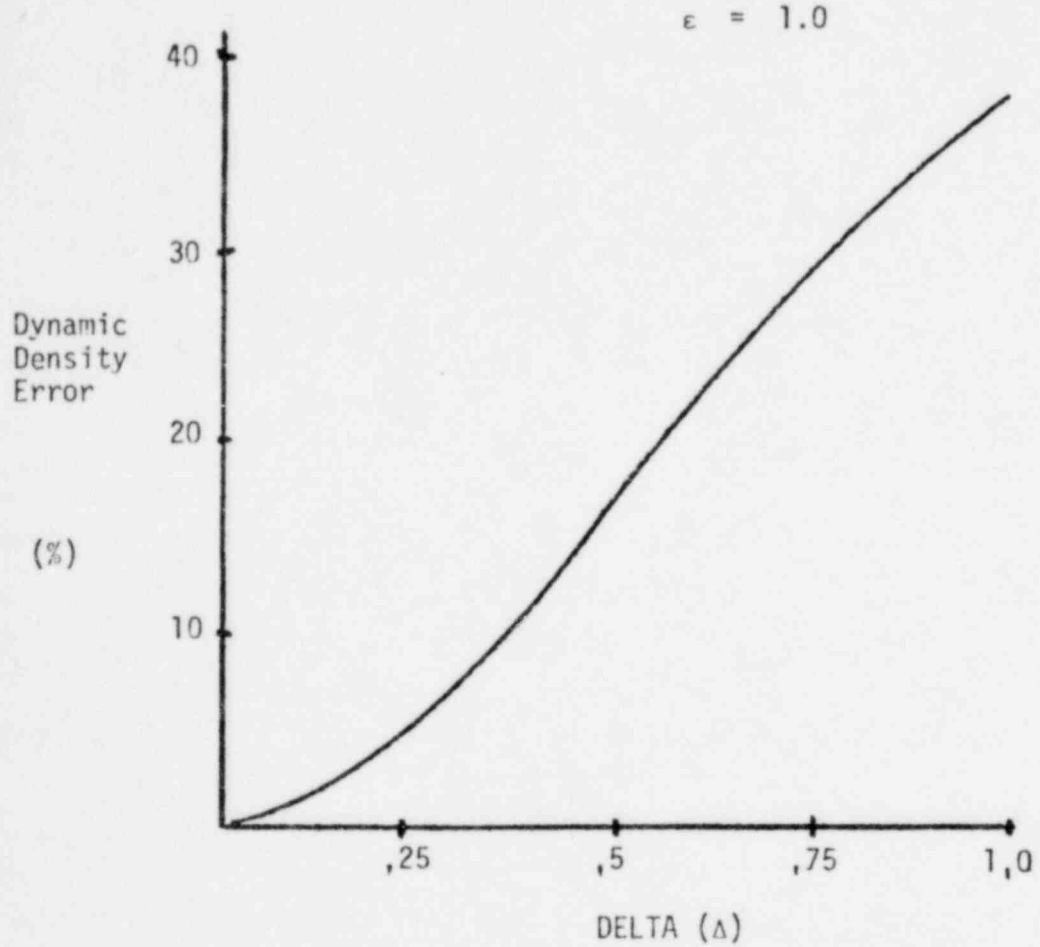

Figure I.2 Dynamic Bias Versus Two-Phase Density Fluctuation Parameter Δ.

$\rho_{sv_o} = 500\ Kg/m^3$

$\rho_{2\phi_o} = 500\ Kg/m^3$

$\Delta = 1.0$

$\varepsilon = 1.0$

$a = b = c = d = 0.25$

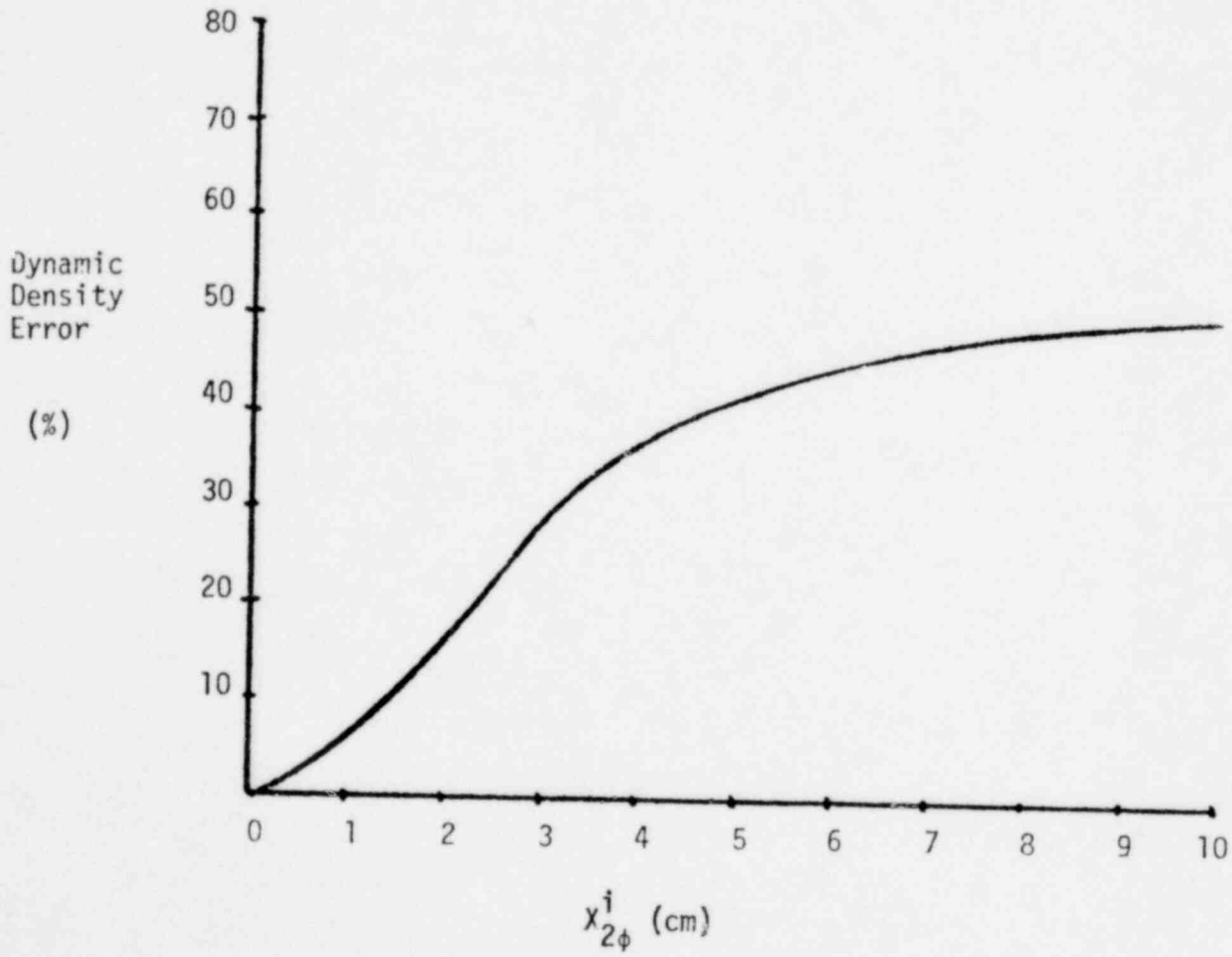

Figure I.3 Dynamic Bias Versus Distance Into Flow Channel

I.3 The Analysis of a Diamond Tipped Optical Probe

In the previous Quarterly Report [5], the ray tracing computer programs for the conical diamond tipped optical probe were summarized. These programs established the optimum geometry for the diamond tip. This may be thought of as having been the development of a kinematic theory of the probe, since no absorption or attenuation had entered into the calculations. Diamond tips were cut and polished to these specifications, and tests made. These data indicated that the purely kinematic model was insufficient, since, due to the many reflections which occured and consequent long paths through the diamond, attenuation was observed to occur. Consequently, the computer model was improved to include absorption along the beam path by Beer's Law, and attenuation on reflection according to Fresnel's equations for reflection, and transmission coefficients as a function of angle of incidence. This may be thought of as the development of the dynamical theory of the diamond probe. These refinements have brought the computer model into agreement with the actual performance of the diamond tipped probe.

I.4 Ultrasonic Measurements in Two-Phase Flow

During the Eleventh Quarter several attempts were made to measure the global void fraction a two-phase mixture. The first attempt was through the use of a pulse-echo (ie: sonar) technique. This proved effective only for situations in which there were few number of bubbles. For most cases of practical significance the scattering and/or resonance attenuation was such that it was not possible to determine the void fraction.

Another technique was the transmission technique. In this technique the signal (pulse) is sent across the channel and picked up by an adjacent transducer. In principle, the attenuation and/or phase-shift of the input signal can then be used to infer void fraction. The experimental setup used is shown in figure I.4. The top set of transducers is intrusive while the bottom set is not.

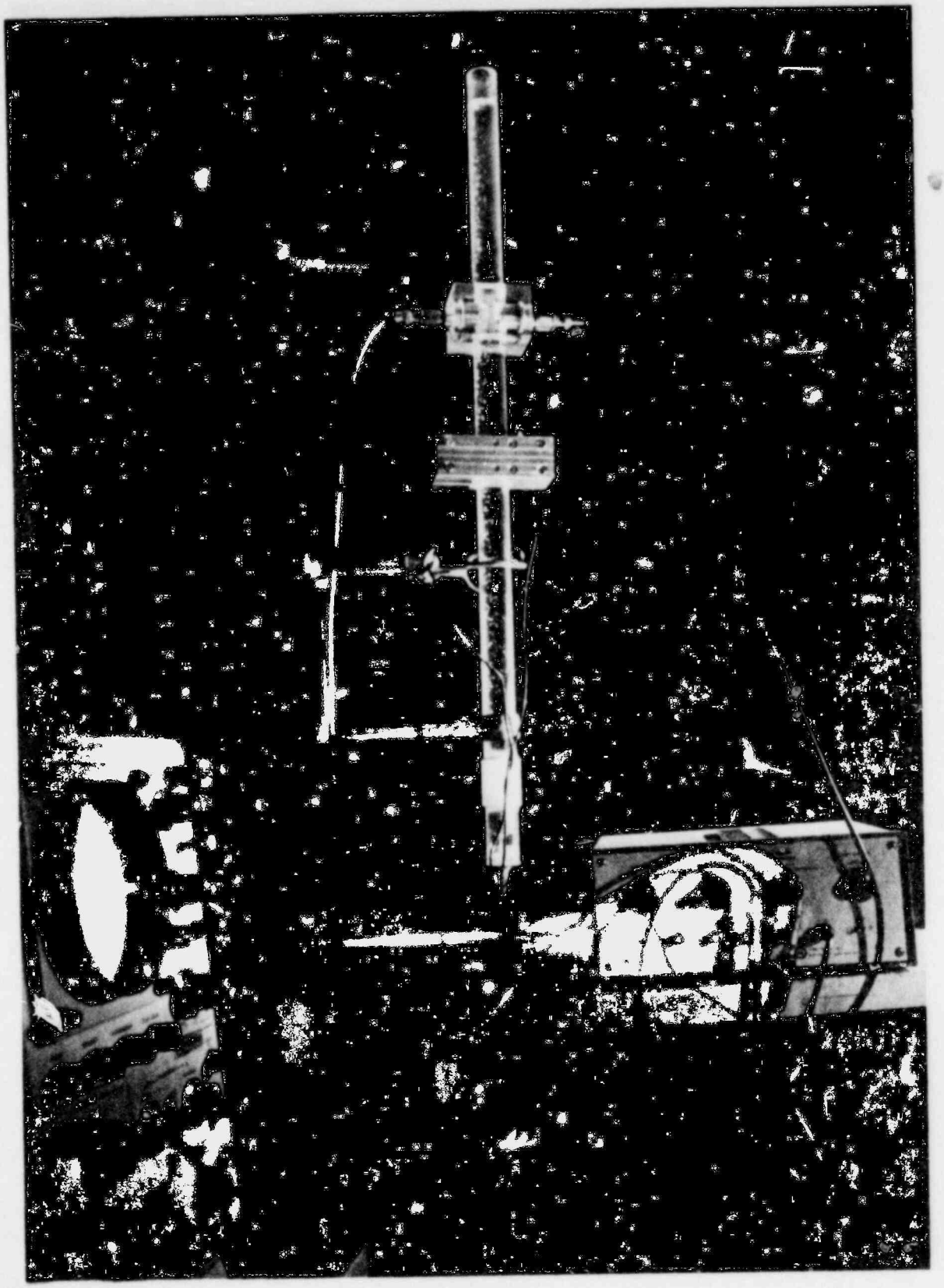

FIGURE I.4

Ultrasonic Measurements
in Two-Phase Flow

It was found that the intrusive arrangement was far superior to the nonintrusive one, due to the fact that the pipe wall introduced considerable attenuation. Preliminary indications were that the measurement of phase-shift would be a more accurate indication of global void fraction than attenuation. Unfortunately sufficiently accurate electronics (to measure phase-shift) were not available with which to accurately measure void fraction.

TASK II

PHASE DISTRIBUTION AND SEPARATION PHENOMENA

Probably the least understood, but most important, aspect of two-phase flow is the multidimensional effects that are exhibited. In particular, our current understanding of phase distribution and separation phenomena is quite primitive. Today, we are still not able to write down the conservation laws which explain why annular flow develops as observed, nor are we able to adequately explain measured subchannel distributions. Moreover, we do not even have empirical correlations for such things as phase stripping in tees and at simple area changes.

The purpose of this task is to address these fundamental problems, both analytically and experimentally.

II.1 Phase Distribution Analysis

In past quarterly reports, we have presented and analyzed a model for phase distribution in a pipe, and compared the predictions of this model with the limited data available. Since these models relate phase distribution to the local turbulence structure of the continuous phase, they are difficult to use in conjunction with current methods for the prediction of two-phase flows.

We have previously [3] used these local models, relating the lateral void distribution to the liquid turbulence structure, to derive an equation which related the cross-sectionally-averaged value of void fraction, to the cross-sectionally averaged mass flux. The result of this derivation was considered suitable for use in predicting the equilibrium phase distribution in current generation subchannel codes. That is, for use as the lateral "void drift" model [6] in subchannel codes using a mixture momentum equation. Unfortunately, some of the codes currently under development use phasic rather than mixture conservation equations, and thus the previous analysis is not directly applicable to them.

Let us now develop a phase distribution model which is suitable for use in predicting the equilibrium phase distribution in codes having phasic conservation equations. Thus we shall relate the cross-sectionally averaged value of $\alpha(x,y)$ to the mass-weighted cross-sectionally averaged phasic velocities (ie: phasic mass fluxes).

We define the cross-sectionally averaged void fraction of subchannel i to be,

$$\langle\alpha\rangle_i = \frac{1}{A_{x-s_i}} \iint_{A_{x-s_i}} \alpha(x,y)\, dxdy \tag{II.1}$$

and the subchannel-average mass flux of phase-k to be,

$$G_{vi} = \langle\alpha\rho_v\, u_{vz}\rangle_i \tag{II.2}$$

$$G_{\ell i} = \langle(1-\alpha)\rho_\ell\, u_{\ell z}\rangle_i \tag{II.3}$$

The subchannel average total mass flux (G_i) is thus,

$$G_i = G_{vi} + G_{\ell i} \tag{II.4}$$

For steady, fully developed flow in geometries of arbitrary cross-section, we have previously [1] derived an expression for the lateral void distribution

$$\frac{\alpha^q(x,y)}{[1-\alpha(x,y)]} = \hat{C}_3\, K_{\ell z}^{1-q}\, e^{(1-q)I(x,y)} \tag{II.5}$$

where $I(x,y)$ is a line integral which quantifies the effect of the non-isotropy of the turbulence on the void distribution. For most cases of practical concern, $q<<1$, and so equation (II.5) reduces to,

$$\alpha(x,y) = 1-\hat{C}_3^{-1}\, K_{\ell z}^{-1}\, e^{-I(x,y)} \tag{II.6}$$

We must now deduce a relationship between the turbulent kinetic energy $K_{\ell z}$, and G_{vi} and $G_{\ell i}$. A convenient approach is suggested by the well-known single-phase relationship, that for a given Reynolds number Re_i, the local velocity fluctuations $u'_{\ell z}$ are proportional to the local mean velocity $u_{\ell z}$. That is, for single-phase flow, at some point c in the subchannel (taken to be the location at which the time-averaged velocity is a maximum),

$$[u'_{\ell z}(x,y)/u_{\ell z}(x,y)]_c = F_{1\phi}(Re_i), \tag{II.7}$$

where,

$$Re_i \triangleq \frac{G_i D_{Hi}}{\mu_\ell}$$

For turbulent two-phase flow, we expect that such a relationship can be expressed as,

$$[u'_{\ell z}(x,y)/u_{\ell z}(x,y)]_c = F_{2\phi}(\langle\alpha\rangle_i, Re_{\ell i} Re_{vi}) \tag{II.8}$$

where,

$$Re_{ki} \triangleq \frac{G_{ki} D_{Hi}}{\mu_k}$$

Equation (II.8) expresses the fact that we expect the turbulence intensity in a two-phase mixture to depend on several factors. First, liquid phase turbulence could be generated by wall shear. This motivates the dependence of $F_{2\phi}$ on $Re_{\ell i}$. This turbulent flow field could be modified by the presence of the vapor phase, thus, we include here a dependence of $F_{2\phi}$ on $\langle\alpha\rangle_i$. We further note that turbulence intensity in the liquid phase can be generated by relative motion between the phases. Thus, we expect $F_{2\phi}$ to depend on $u_{r_i} = u_{vz_i} - u_{\ell z_i}$, where

$$u_{kz_i} \triangleq \frac{G_{k_i}}{\langle\alpha_k\rangle_i \rho_k}$$

However, since $F_{2\phi}$ is dimensionless, u_{r_i} must be included in a dimensionless fashion. This is effectively done by allowing $F_{2\phi}$ to depend on G_{v_i}, G_{ℓ_i} and $\langle\alpha\rangle_i$ through Re_{v_i}, Re_{ℓ_i}, and $\langle\alpha\rangle_i$.

Let us now assume,

$$K_{\ell z} \triangleq \frac{1}{2}\rho_\ell (u'_{\ell z})^2 = \frac{1}{2}\rho_\ell (u'_{\ell z})_c^2 \, f_1^2(x,y;G_{v_i},G_{\ell_i},\langle\alpha\rangle_i) \tag{II.9}$$

or, using (II.8), we have,

$$K_{\ell z} = \frac{1}{2}\rho_\ell (u_{\ell z})_c^2 \, F_{2\phi}^2 \, (Re_{v_i},Re_{\ell_i},\langle\alpha\rangle_i) \, f_1^2 \, (x,y;G_{v_i},G_{\ell_i},\langle\alpha\rangle_i) \tag{II.10}$$

We can now combine equations (II.6) and (II.10), and average over the flow area of subchannel-i, to obtain,

$$\langle\alpha\rangle_i = 1\text{-}2\,\hat{C}_3^{-1}\,\rho_\ell^{-1}(u_{\ell z})_c^{-2}\,F_{2\phi}^{-2}\,(Re_{v_i},Re_{\ell_i},\langle\alpha\rangle_i)A_i \tag{II.11}$$

where,

$$A_i(G_{v_i},G_{\ell_i},\langle\alpha\rangle_i) \triangleq \left\langle f_1^{-2}(x,y;Re_{v_i},Re_{\ell_i},\langle\alpha\rangle_i)\, e^{-I(x,y)} \right\rangle_i \tag{II.12}$$

It should be noted that all details (ie: profile effects) of the turbulent structure are contained in A_i.

We now wish to obtain a relationship between $(u_{\ell z})_c$, G_{ℓ_i} and $\langle\alpha\rangle_i$. It is convenient to define,

$$u_{\ell z}(x,y) \triangleq (u_{\ell z})_c \, f_2(x,y;G_{v_i},G_{\ell_i},\langle\alpha\rangle_i) \tag{II.13}$$

and,

$$\alpha(x,y) \triangleq \langle\alpha\rangle_i \, f_3(x,y,G_{v_i},G_{\ell_i},\langle\alpha\rangle_i) \tag{II.14}$$

combining equation (II.13) and (II.14) with equation (II.3) gives,

$$G_{\ell_i} = B_i(G_{v_i},G_{\ell_i},\langle\alpha\rangle_i)\,(u_{\ell z})_c - C_i(G_{v_i},G_{\ell_i},\langle\alpha\rangle_i)\langle\alpha_i\rangle(u_{\ell z})_c \tag{II.15}$$

where,

$$B_i(G_{v_i}, G_{\ell_i}, \langle\alpha\rangle_i) \triangleq \rho_\ell \langle f_2(x,y;G_{v_i}, G_{\ell_i}, \langle\alpha\rangle_i) \tag{II.16a}$$

$$C_i(G_{v_i}, G_{\ell_i}, \langle\alpha\rangle_i) \triangleq \rho_\ell \langle f_2(x,y;G_{v_i}, G_{\ell_i}, \langle\alpha\rangle_i) \quad f_3(x,y,G_{v_i}, G_{\ell_i}, \langle\alpha\rangle_i)\rangle \tag{II.16b}$$

Thus, from equation (II.15) we have,

$$(u_{\ell z})_c = \frac{G_{\ell_i}}{[B_i - C_i \langle\alpha\rangle_i]} \tag{II.17}$$

Using equation (II.17) in (II.11) gives,

$$\langle\alpha\rangle_i = 1 - \hat{C}_3^{-1} \rho_\ell^{-1} F_{2\phi}^{-2} (Re_{v_i}, Re_{\ell_i}, \langle\alpha\rangle_i) A_i G_{\ell_i}^{-2} (B_i - C_i \langle\alpha\rangle_i)^2 \tag{II.18}$$

Thus, within this formulation, the role of the void distribution relationship in equation (II.5) is to provide the functional relationship between $\langle\alpha\rangle_i$, G_{v_i} and G_{ℓ_i}, which is given by equation (II.18). To evaluate equation(II.18), and determine the explicit relationship between $\langle\alpha\rangle_i$, G_{v_i} and G_{ℓ_i},requires knowledge of the distribution parameters A_i, B_i, and C_i, and the function $F_{2\phi}$, and the constant $\hat{C}_3$. In general, we do not know these quantities as functions of $\langle\alpha\rangle_i$, G_{v_i}, and G_{ℓ_i}. Due to our lack of knowledge, we shall expand equation (II.18) about the bundle-average liquid and vapor mass fluxes, $\bar{G}_\ell$ and $\bar{G}_v$. and the bundle average void fraction $\langle\bar{\alpha}\rangle$. To simplify the calculation, we can write equation (II.18) in the form,

$$H_i(\langle\alpha\rangle_i, G_{v_i}, G_{\ell_i}) = 0 \tag{II.19}$$

Thus, we have,

$$\langle\alpha\rangle_i = \overline{\langle\alpha\rangle} + (\langle\alpha\rangle_i - \overline{\langle\alpha\rangle}) \triangleq \overline{\langle\alpha\rangle} + \Delta\langle\alpha\rangle_i \tag{II.20a}$$

$$G_{k_i} = \bar{G}_k + (G_{k_i} - \bar{G}_k) \triangleq \bar{G}_k + \Delta G_{k_i} \tag{II.20b}$$

Substituting equations (II.20) into (II.19) gives,

$$H_i(\langle\bar{\alpha}\rangle+\Delta\langle\alpha\rangle_i,\bar{G}_v + \Delta G_{v_i},\bar{G}_\ell + \Delta G_{\ell_i}) = 0$$

$$\cong H_i(\langle\bar{\alpha}\rangle,\bar{G}_v,G_\ell) + \frac{\partial H_i}{\partial\langle\alpha\rangle_i}\ (\langle\bar{\alpha}\rangle,\bar{G}_v,\bar{G}_\ell)\ \Delta\langle\alpha\rangle_i + \frac{\partial H_i}{\partial G_{v_i}}\ (\langle\alpha\rangle,\bar{G}_v,\bar{G}_\ell)\ \Delta G_{v_i}$$

$$+ \frac{\partial H_i}{\partial G_{\ell i}}\ (\langle\bar{\alpha}\rangle,\ \bar{G}_v,\bar{G}_\ell)\ \ \Delta G_{\ell_i} \qquad \text{(II.21)}$$

If we define:

$$H_i(\langle\bar{\alpha}\rangle,\bar{G}_v,\bar{G}_\ell) \triangleq D_i \qquad \text{(II.22a)}$$

$$\frac{\partial H_i}{\partial\langle\alpha\rangle_i}\ (\langle\bar{\alpha}\rangle,\bar{G}_v,\ \bar{G}_\ell) \triangleq E_i \qquad \text{(II.22b)}$$

$$\frac{\partial H}{\partial G_{v_i}}\ (\langle\bar{\alpha}\rangle,\bar{G}_v,\bar{G}_\ell) \triangleq F_i \qquad \text{(II.22c)}$$

$$\frac{\partial H}{\partial G_{\ell_i}}\ (\langle\bar{\alpha}\rangle,\bar{G}_v,\bar{G}_\ell) \triangleq J_i \qquad \text{(II.22d)}$$

Equation (II.21) becomes,

$$D_i + E_i\ \ \Delta\langle\alpha\rangle_i + F_i\ \ \Delta G_{v_i} + J_i\ \ \Delta G_{\ell_i} = 0 \qquad \text{(II.23)}$$

Solving for $\Delta\langle\alpha\rangle_i$ gives

$$\Delta\langle\alpha\rangle_i = -\frac{D_i}{E_i} - \frac{F_i}{E_i}\ \ \Delta G_{v_i} - \frac{J_i}{E_i}\ \ \Delta G_{\ell_i} \qquad \text{(II.24)}$$

which can also be written as,

$$\Delta\langle\alpha\rangle_i = M_i + N_i\ \Delta G_{v_i} + P_i\ \Delta G_{\ell_i} \qquad \text{(II.25)}$$

Equation (II.25) gives the relationship which quantifies the variation of the void fraction of subchannel-i with respect to the bundle average void fraction, in terms of the variations of the subchannel vapor and liquid phase mass fluxes, with respect to their bundle average values.

Let us now examine equation (II.25) for adjoining subchannels. Let us write equation (II.25) for two adjoining subchannels i and j,

$$\Delta\langle\alpha\rangle_i = M_i + N_i \Delta G_{v_i} + P_i \Delta G_{\ell_i} \tag{II.26}$$

$$\Delta\langle\alpha\rangle_j = M_j + N_j \Delta G_{v_j} + P_j \Delta G_{\ell_j} \tag{II.27}$$

Subtracting equation (II.27) from (II.26) gives,

$$\Delta\langle\alpha\rangle_i - \Delta\langle\alpha\rangle_j = \langle\alpha\rangle_i - \langle\alpha\rangle_j = M_i - M_j + N_i \Delta G_{vi} - N_j \Delta G_{v_j}$$

$$+ P_i \Delta G_{v_i} - P_j \Delta G_{v_j} \tag{II.28}$$

The definitions of ΔG_{k_i} can be used to write (II.28) in the form,

$$\langle\alpha\rangle_i - \langle\alpha\rangle_j = M_i - M_j + \frac{(N_i+N_j)}{2}(G_{v_i} - G_{v_j}) + \frac{(P_i+P_j)}{2}(G_{\ell_i} - G_{\ell_j})$$

$$+ (N_i - N_j)\left[\frac{G_{v_i}+G_{v_j}}{2} - \bar{G}_v\right] + (P_i - P_j)\left[\frac{G_{\ell_i}+G_{\ell_j}}{2} - \bar{G}_\ell\right] \tag{II.29}$$

Previously published expressions for void drift [3], [6] involve $\langle\alpha\rangle_i - \langle\alpha\rangle_j$ and the <u>total</u> mass fluxes of subchannels i and j, G_i and G_j. In contrast, equation (II.29) is more general since it involves the phasic mass fluxes for subchannels i and j, G_{v_i}, G_{v_j}, G_{ℓ_i}, G_ℓ It is interesting to note that if $N_i = P_i$ and $N_j = P_j$, equation (II.29) formally becomes the same as that derived previously [3], involving G_i and G_j.

We can view equation (II.29) as a physically based result which can be reduced to previous [6] "void drift" models. Thus, equation (II.29) provides an analytical justification for empirical "void drift" models. Furthermore, it provides a means of obtaining a more exact relationship for the equilibrium void expression needed in advanced subchannel models.

During the Eleventh Quarter we also devoted considerable effort to the assembly of the finite element equations for the two-dimensional test section shown schematically in figure II.1a.

Recall that we had constructed a Galerkin formulation of the problem by multiplying each of the governing partial differential equations of phasic continuity and momentum by an appropriate weight function and integrating over the flow domain([7], equations (II.11-16)). Next, the flow variables (velocity components, pressure, and void fraction) were approximated in terms of piecewise bilinear trial functions([5], equations (II.19,20))and the weight functions were approximated by piecewise bi-quadratic "upwind" test functions([5], equations (II.21, 22, 24)). Substituting these approximations into the Galerkin integrals we found their contribution on a single element to have the form ([5],equations (II.25)) of,

(1) vapor phase continuity

$$\delta \underset{\sim}{a}_e^{\alpha} \left(K_1^e \underset{\sim}{a}_e^{v} + K_2^e \underset{\sim}{a}_e^{\alpha}\right) = 0 \qquad \text{(II.30a)}$$

(2) liquid phase continuity

$$\delta \underset{\sim}{a}_e^{p} \left(K_3^e \underset{\sim}{a}_e^{\ell} - K_2^e \underset{\sim}{a}_e^{\alpha}\right) = 0 \qquad \text{(II.30b)}$$

(3) vapor phase momentum

$$\delta \underset{\sim}{a}_e^{v} [(K_5^e + K_7^e) \underset{\sim}{a}_e^{v} - K_7^e \underset{\sim}{a}_e^{\ell} + K_6^e \underset{\sim}{a}_e^{p} + K_9^e] = 0 \qquad \text{(II.30c)}$$

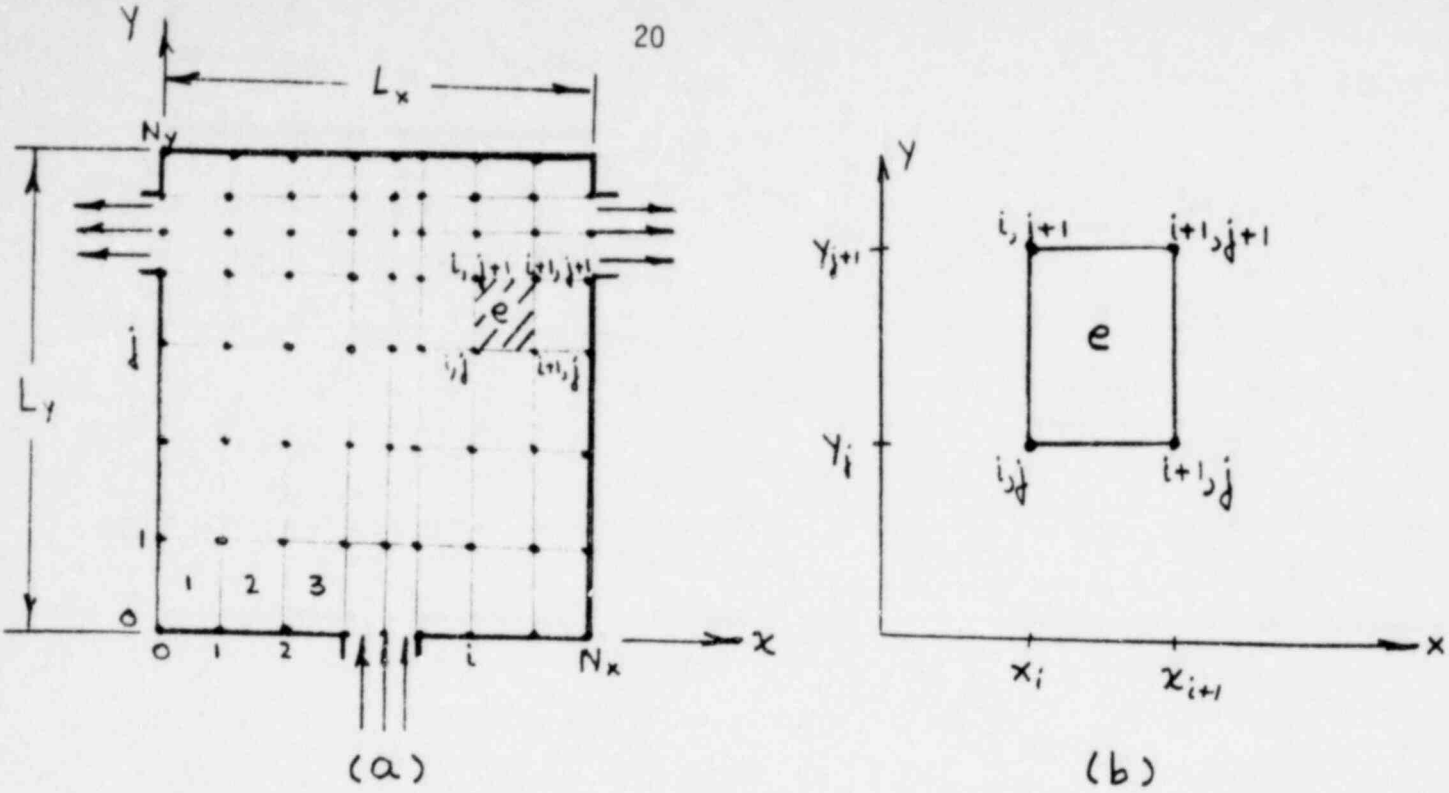

(a) FLOW DOMAIN AND NODE NUMBERING FOR THE CHANNEL AND (b) NODAL GEOMETRY OF A SINGLE ELEMENT, SAY, ELEMENT NO. e.

FIGURE II.1

FINITE ELEMENT GRID FOR
2-D TEST SECTION

(4) liquid phase momentum

$$\delta \underset{\sim}{a}^{\ell}_{e} \left[-K^{e}_{7}\, \underset{\sim}{a}^{v}_{e} + (K^{e}_{15} + K^{e}_{7})\, \underset{\sim}{a}^{\ell}_{e} + K^{e}_{16}\, a^{p}_{e} + K^{e}_{19}\right] = 0 \qquad \text{(II.30d)}$$

where, ($k = \ell, v$)

$$[\underset{\sim}{a}^{k}_{e}]^{T} \triangleq [u^{k}_{i,j} v^{k}_{i,j} u^{k}_{i+1,j}\ v^{k}_{i+1,j}\ u^{k}_{i,j+1}\ v^{k}_{i,j+1}\ u^{k}_{i+1,j+1}\ v^{k}_{i+1,j+1}] \qquad \text{(II.31a)}$$

$$[\underset{\sim}{a}^{p}_{e}]^{T} \triangleq [p_{i,j} p_{i+1,j}\ p_{i,j+1}\ p_{i+1,j+1}] \qquad \text{(II.31b)}$$

$$[\underset{\sim}{a}^{\alpha}_{e}]^{T} \triangleq [\alpha_{i,j}\, \alpha_{i+1,j}\ \alpha_{i,j+1}\ \alpha_{i+1,j+1}]. \qquad \text{(II.31c)}$$

The vectors $\underset{\sim}{a}^{v}_{e}$, $\underset{\sim}{a}^{\ell}_{e}$, $\underset{\sim}{a}^{p}_{e}$, $\underset{\sim}{a}^{\alpha}_{e}$ store the unknown vapor phase velocity vectors $[u^{v}_{rs}\ v^{v}_{rs}]^{T}$, liquid phase velocity vectors $[u^{\ell}_{rs}\ v^{\ell}_{rs}]^{T}$, pressures p_{rs}, and void fractions α_{rs}, respectively, at the four nodes (r,s=i,j;i+1,j;i,j+1,i+1,j+1) of element number-e shown in Figure II.1b. The vectors δa^{v}_{e}, δa^{ℓ}_{e}, δa^{p}_{e}, δa^{α}_{e} store the "virtual",vapor phase velocity vectors $[\delta u^{v}_{rs}, \delta v^{v}_{rs}]^{T}$, liquid phase velocity vectors $[\delta u^{\ell}_{rs}, \delta v^{\ell}_{rs}]^{T}$, pressures δp_{rs}, and void fractions $\delta\alpha_{rs}$, respectively,at the four nodes of element number-e. The virtual quantities are defined by relations analogous to equations (II.31). The K^{e}_{r}'s are matrices* of integrals over element-e involving the trial functions, test functions, and $\underset{\sim}{a}^{v}_{e}$, $\underset{\sim}{a}^{\ell}_{e}$, $\underset{\sim}{a}^{p}_{e}$, and $\underset{\sim}{a}^{\alpha}_{e}$.

The assembly process consists of summing equations (II.30) over all elements. Thus, we have:

(1) vapor phase continuity,

$$\sum_{e=1}^{N} \delta a^{\alpha}_{e} \left[K^{e}_{1}\, \underset{\sim}{a}^{v}_{e} + K^{e}_{2}\, \underset{\sim}{a}^{\alpha}_{e}\right] = 0 \qquad \text{(II.32a)}$$

*Some of the K^{e}_{i}'s in equations (II.30) were redefined from those in [5] (equations (II.25)) in order to simplify the presentation.

(2) liquid phase continuity

$$\sum_{e=1}^{N} \delta a_e^p \left[K_3^e \underset{\sim}{a}_e^{\ell} - K_2^e \underset{\sim}{a}_e^{\alpha} \right] = 0 \qquad \text{(II.32b)}$$

(3) vapor phase momentum,

$$\sum_{e=1}^{N} \delta a_e^v \left[(K_5^e + K_7^e) \underset{\sim}{a}_e^v - K_7^e \underset{\sim}{a}_e^{\ell} + K_6^e \underset{\sim}{a}_e^p + K_9^e \right] = 0 \qquad \text{(II.32c)}$$

(4) liquid phase momentum,

$$\sum_{e=1}^{N} \delta a_e^{\ell} \left[-K_7^e \underset{\sim}{a}_e^v + (K_{15}^e + K_7^e) \underset{\sim}{a}_e^{\ell} + K_{16}^e \underset{\sim}{a}_e^p + K_{19}^e \right] = 0 \qquad \text{(II.32d)}$$

where N is the total number of finite elements in the problem. Notice that the flow variables, u_{ij}^v, v_{ij}^v, u_{ij}^{ℓ}, v_{ij}^{ℓ}, p_{ij}, α_{ij}, associated with node i,j can appear in at most four terms in the sums of equations (II.32); namely for those elements, shown in figure II.2, which contain node i,j.

The finite element equations are obtained by invoking the Principle of Virtual Work, which states that when a flow variable is not prescribed (ie: not specified by a boundary condition) then equations (II.32) should be satisfied for any and all possible values of the virtual flow variables. This implies that the finite element equations associated with a node i,j lying in the interior of the channel, and not on solid walls or inlets and outlets, must have the form,

$$\sum_{r=i-1}^{i+1} \sum_{s=j-1}^{j+1} C_{ij}^{rs} \underset{\sim}{a}_{rs} = \underset{\sim}{b}_{ij}, \qquad \text{(II.33)}$$

where,

$$\underset{\sim}{a}_{rs} = [u_{rs}^v \; v_{rs}^v \; u_{rs}^{\ell} \; v_{rs}^{\ell} \; p_{rs} \; \alpha_{rs}]. \qquad \text{(II.34)}$$

The matrices C_{ij}^{rs} and vectors $\underset{\sim}{b}_{ij}$ are obtained by adding appropriate rows and columns of the K_r^e matrices for the four elements surrounding node i,j. The

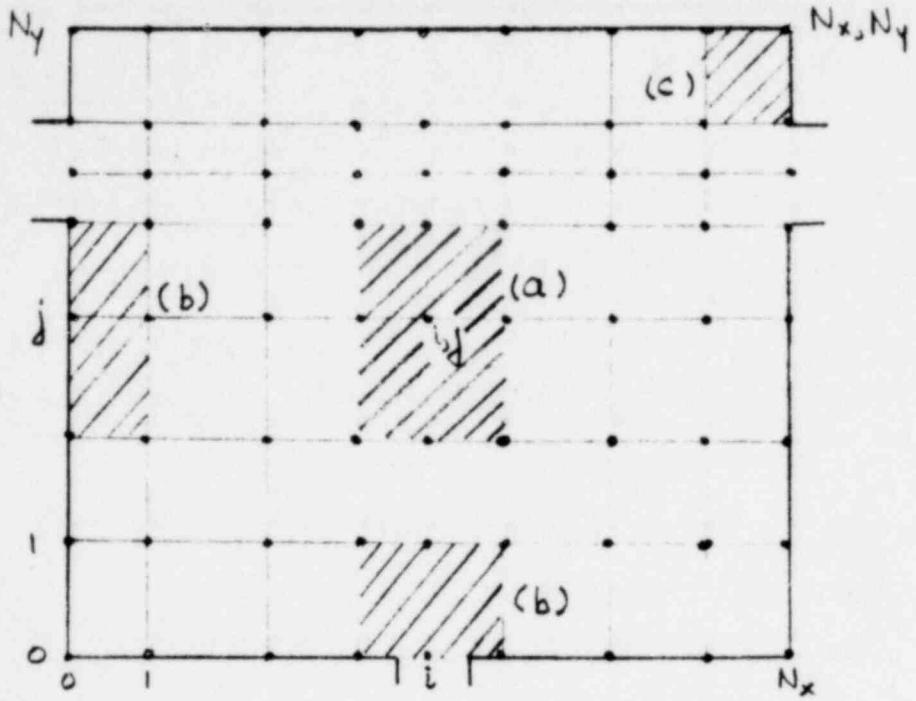

(a) SUPPORT OF A NODE i,j INTERIOR TO THE CHANNEL INVOLVES THE FOUR NEIGHBORING ELEMENTS.

(b) SUPPORT OF A NODE ON A SOLID WALL (E.G. 0,j) OR IN AN INLET (E.G. i,0) OR OUTLET INVOLVES THE TWO NEIGHBORING ELEMENTS.

(c) SUPPORT OF A CORNER NODE (E.G. N_x, N_y) INVOLVES ONLY ONE ELEMENT.

FIGURE II.2
VARIOUS FINITE ELEMENT
NODES

detailed structure of the C_{ij}^{rs} and $\underset{\sim}{b}_{ij}$ is algebraically complicated and for that reason we have not presented their precise definitions here. However, the C_{ij}^{rs} and $\underset{\sim}{b}_{ij}$ may be easily generated on a computer by following standard techniques [8],and we have written FORTRAN subroutines to do this. Suffice it to say that each C_{ij}^{rs} is a 6 X 6 matrix and each $\underset{\sim}{b}_{ij}$ is a 6 X 1 vector. The first four rows of C_{ij}^{rs} and $\underset{\sim}{b}_{ij}$ contain momentum equations obtained from equations (II.32c) and (II.32d) and the last two rows contain continuity equations,obtained from equations (II.32a) and (II.32b). Note too that the vector $\underset{\sim}{a}_{rs}$ stores the six unknowns.

Equations (II.33) are not applicable for nodes i,j that lie on solid walls, in inlets, or outlets since some of the flow variables are constrained by boundary conditions there. In particular the following boundary conditions are imposed at nodes lying on solid walls, inlets, or outlets:

$$u_{ij}^{v} = v_{ij}^{v} = u_{ij}^{\ell} = v_{ij}^{\ell} = 0; \text{ if i, j is on a solid wall} \qquad \text{(II.35a)}$$

$$u_{ij}^{v} = u_{ij}^{\ell} = 0; \ \alpha_{ij}\, v_{ij}^{v},\ (1-\alpha_{ij})\, v_{ij}^{\ell} \text{ prescribed;if i,j is at the inlet} \qquad \text{(II.35b)}$$

$$v_{ij}^{v} = v_{ij}^{\ell} = 0; \ p_{ij} \text{ prescribed; if i,j is at an outlet} \qquad \text{(II.35c)}$$

The Principle of Virtual Work states that when a flow variable is prescribed at a node the corresponding virtual flow variable is zero there. Thus, for nodes on solid walls all of the virtual velocities are zero and only the continuity equations should be assembled at these nodes. The finite element equations for a node, o,j (see Figure II.2) lying on the solid wall along the y-axis would have the form,

$$\sum_{r=0}^{1} \sum_{s=j-1}^{j+1} C_{oj}^{rs}\ \underset{\sim}{a}_{rs} = \underset{\sim}{b}_{oj} \qquad \text{(II.36)}$$

FINITE ELEMENT CODE

FOR SOLVING THE 6 EQUATION MODEL
(Two-Dimensional Test Section)

START

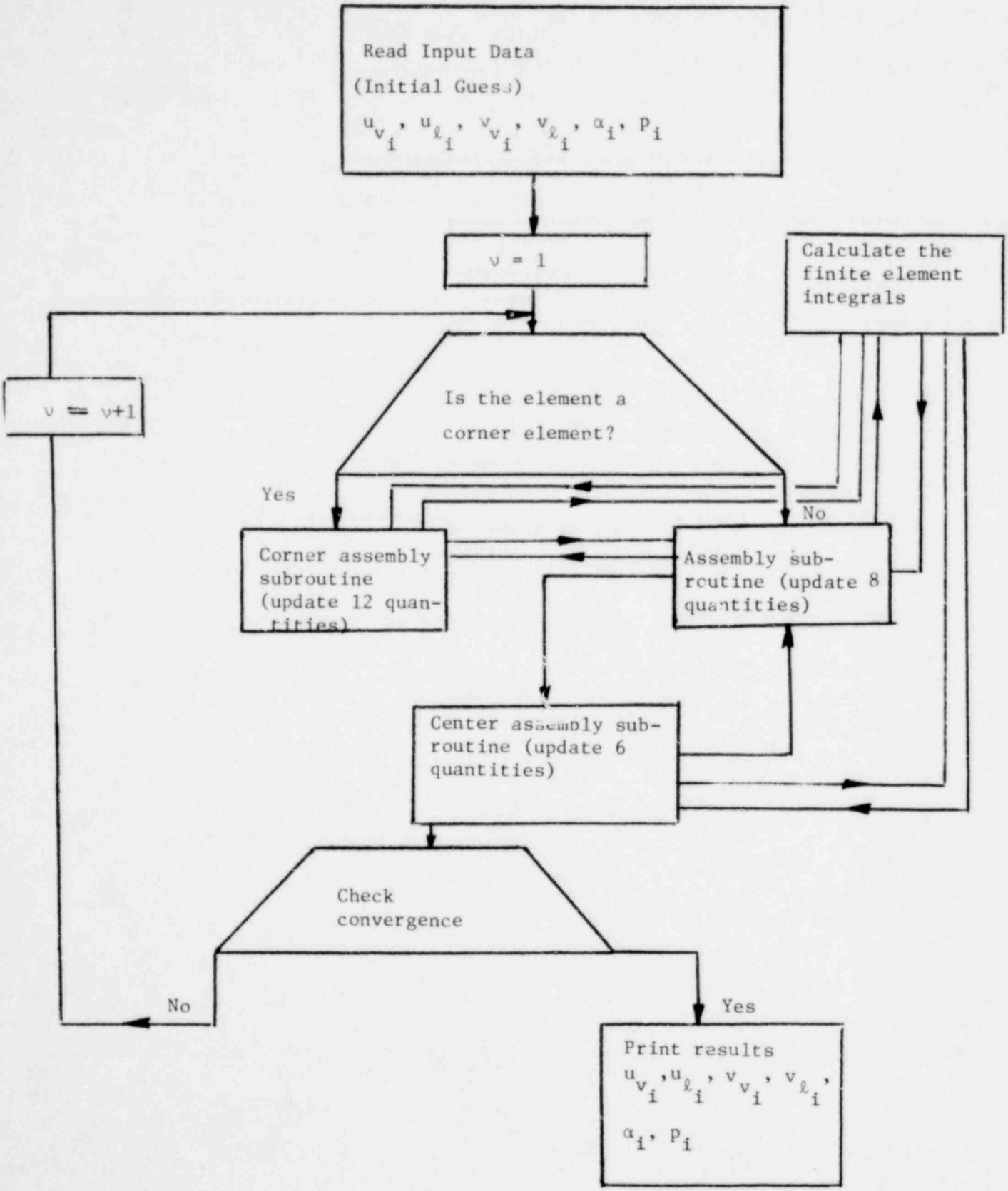

FIGURE II.3

where C_{oj}^{rs} is now a 2 X 6 matrix and $\underset{\sim}{b}_{oj}$ is a 2-element vector, since only the two continuity equations (II.32a,b) are assembled. Similar equations are obtained at other nodes on solid walls. Note that the corner nodes o,o; N_x, o; o, N_y; and N_x, N_y will only involve unknowns on one element (see Figure II.2).

Nodes lying on the flow boundaries but in the inlets or outlets require additional special treatment. We are currently implementing the assembly of these nodes and will report on results in the next quarterly report.

Subsequent to the assembly phase we must solve the finite element equations (II.33-II.36) for the unknown $\underset{\sim}{a}_{ij}$'s at the nodes. A nonlinear SOR routine is being investigated for this task. An overall flow diagram of the assembly and solution process is shown in figure II.3.

II.2 The Analysis of Phase Separation in Tees and Wyes

It has been demonstrated experimentally [9] that the two phases in a two-phase mixture separate unevenly into the downstream branches of tees and wyes. The objective of the work done during the Eleventh Quarter was to develop a predictive model with which one can calculate the distribution of the two-phase mixtures in the two downstream branches of a tee or wye.

Referring to figure II.4, we can note that the nine (9) unknowns for such a flow system are:

Flows: W_1, W_2, W_3 (II.37a)

Qualities: x_1, x_2, x_3 (II.37b)

Pressure drops: Δp_{1-2}, Δp_{1-3} (II.37c)

These unknowns are interrelated through the conservation laws. If a sufficient number of the unknowns are specified, the rest can be calculated from the appropriate conservation equations. Naturally, the number of unknowns specified and the number of conservation equations used must equal to the total number of unknowns.

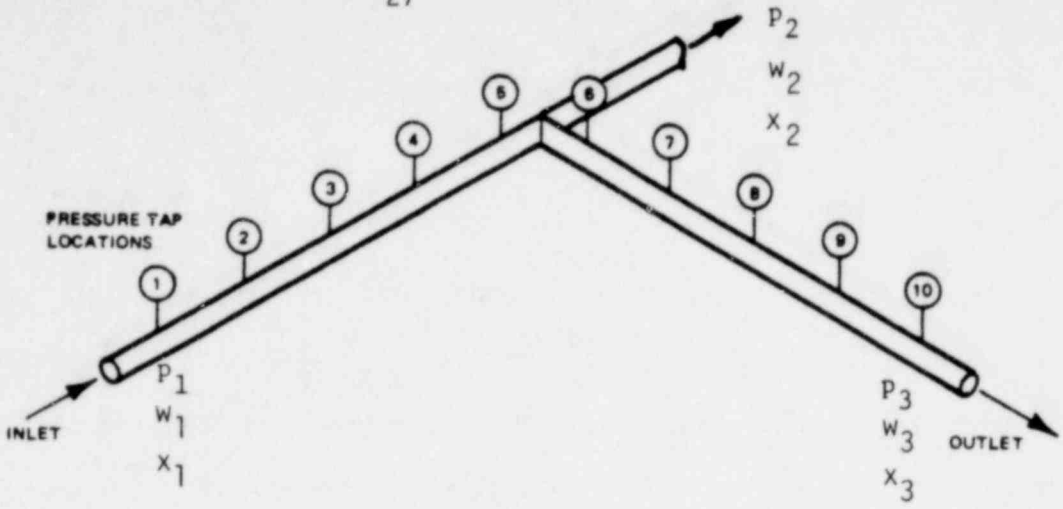

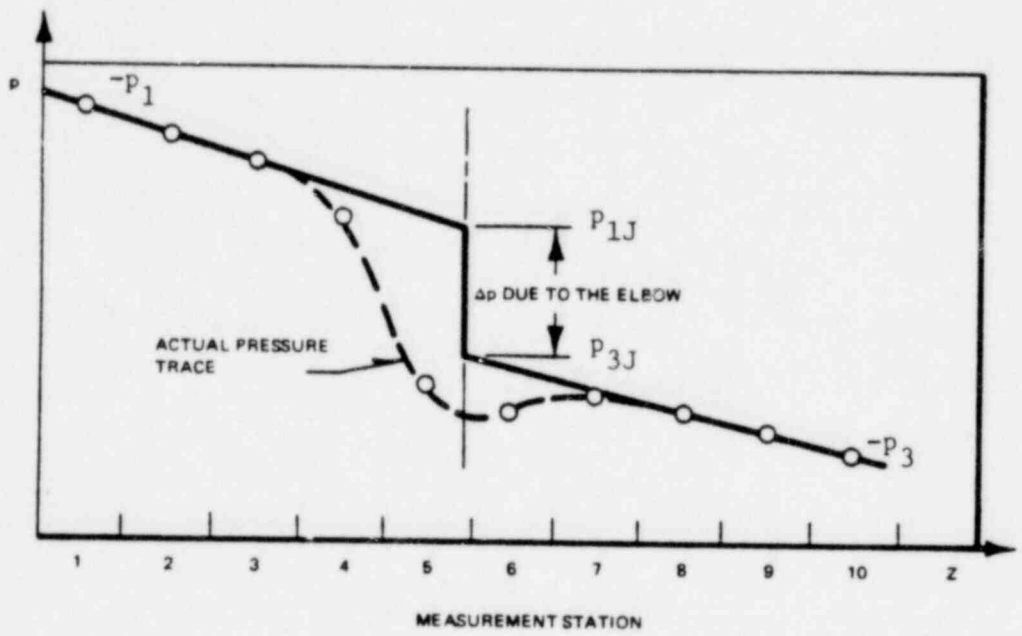

Pressure Profiles in a Tee

FIGURE II.4

In the following analysis, three (3) parameters will be specified. They are:

x_1, Δp_{1-2}, and Δp_{1-3}

Thus, for closure we need five (5) independent conservation equations. The conservation equations which we used were, the mixture continuity equation, the vapor-phase continuity equation, the mixture momentum equation for the branching flow, the mixture momentum equation for the straight run, and the vapor-phase momentum equation for the branching flow. We will now consider these equations one-at-a-time.

Mixture Continuity Equation

$$W_1 = W_2 + W_3 \tag{II.38}$$

where the subscripts 1, 2, and 3 refer to the fully recovered conditions at the inlet section, straight run section and the side branch, respectively.

Vapor-Phase Continuity Equation

$$x_1 W_1 = x_2 W_2 + x_3 W_3 \tag{II.39}$$

In order to further describe the split of the mixture flow, we need two mixture momentum equations, one for the branching flow, and the other for the straight run. These two mixture momentum equations are used to correlate pressure drops across a tee or wye junction. For the pressure drop in the branch, we have,

$$\Delta p_{1-3} = p_1 - p_3 = p_1 - p_{1J} + \Delta p_T + p_{3J} - p_3 \tag{II.40}$$

where, $p_1 - p_{1J}$ represents the pressure loss in the inlet section.

Δp_T represents the pressure loss due to the turning of the mixture into a side branch.

$p_{3J}-p_3$ represents the pressure loss in the side branch, downstream of the junction.

All pressure losses are irreversible losses due to friction and viscous dissipation effects.

To constitute the various pressure losses let us consider a typical single-phase static pressure profile in a pipe fitting, such as a tee or an elbow.

From figure II.4 we see that $\Delta p_T = p_{1J} - P_{3J}$ represents the irreversible pressure loss due to the fluid turning. We can also conclude that the pressure losses in the inlet and side branch section are due to wall shear and gravity. The three components of pressure loss from station-1 to station-3 are given by the following equations,

$$p_1 - p_{1J} = \frac{1}{2g_c} \frac{G_1^2}{\rho_\ell} K_1 \phi_{\ell o_1}^2 + \bar{\rho}_1 \frac{g}{g_c} L_1 \sin\theta \qquad \text{(II.41)}$$

$$p_{3J} - p_3 = \frac{1}{2g_c} \frac{G_3^2}{\rho_\ell} K_3 \phi_{\ell o_3}^2 + \bar{\rho}_3 \frac{g}{g_c} L_3 \sin\theta \qquad \text{(II.42)}$$

where,

$$K_i \overset{\Delta}{=} f_i \, L_i/D_i \qquad \text{(II.43)}$$

f_i = Darcy-Weisbach friction factor

L_i = length of section-i (i = 1,3)

$\phi_{\ell o_i}^2$ = two-phase multiplier in section-i

D_i = hydraulic diameter of section-i

$\bar{\rho}_i \overset{\Delta}{=} (1-\langle\alpha_i\rangle)\, \rho_\ell + \langle\alpha_i\rangle \rho_v$

and for convenience we have assumed a homogeneous multiplier,

$$\phi_{\ell o_i}^2 = \left(1 + \frac{v_{\ell v}}{v_\ell} x_i\right)$$

For the turning loss, Δp_T, we can use Chisholm's model [10], which is given by,

$$\Delta p_T = p_{1J} - p_{3J} = \frac{1}{2g_c} \frac{G_1^2}{\rho_\ell} \zeta_{1-3} (1-x_1)^2 \left[1 + \frac{C}{X_{tt}} + \frac{1}{X_{tt}^2}\right] \tag{II.46}$$

where,

$$\frac{1}{X_{tt}} = \left(\frac{x_1}{1-x_1}\right)\left(\frac{\rho_\ell}{\rho_v}\right)^{1/2} \tag{II.47}$$

and,

$$C = \left\{1 + (C_3-1)\left(\frac{\rho_\ell-\rho_v}{\rho_\ell}\right)^{1/2}\right\}\left\{\left(\frac{\rho_\ell}{\rho_v}\right)^{1/2} + \left(\frac{\rho_v}{\rho_\ell}\right)^{1/2}\right\} \tag{II.48}$$

The suggested value [10] for C_3 is 1.75. ζ_{1-3} is the single phase loss coefficient for a tee/wye junction, given by,

$$\zeta_{1-3} = \zeta_{1-3}\left(\frac{A_3}{A_1}, \frac{G_3}{G_1}\right) \tag{II.49}$$

Curves for ζ_{1-3} have been given by Miller [11]. Two examples of such curves are plotted in figure II.5, one for a 90° tee and the other for a 45° tee. While not specifically tested, the orientation of a tee might be expected to affect the values of ζ_{1-3}.

In a similar manner, for the pressure loss in the straight run portion of a tee/wye we can assume it to be made up of three components: that due to the inlet section, the junction, and the downstream section. Specifically

$$\Delta p_{1-2} = p_1 - p_2 = (p_1 - p_{1J}) + (\Delta p_J) + (p_{2J} - p_2) \tag{II.50}$$

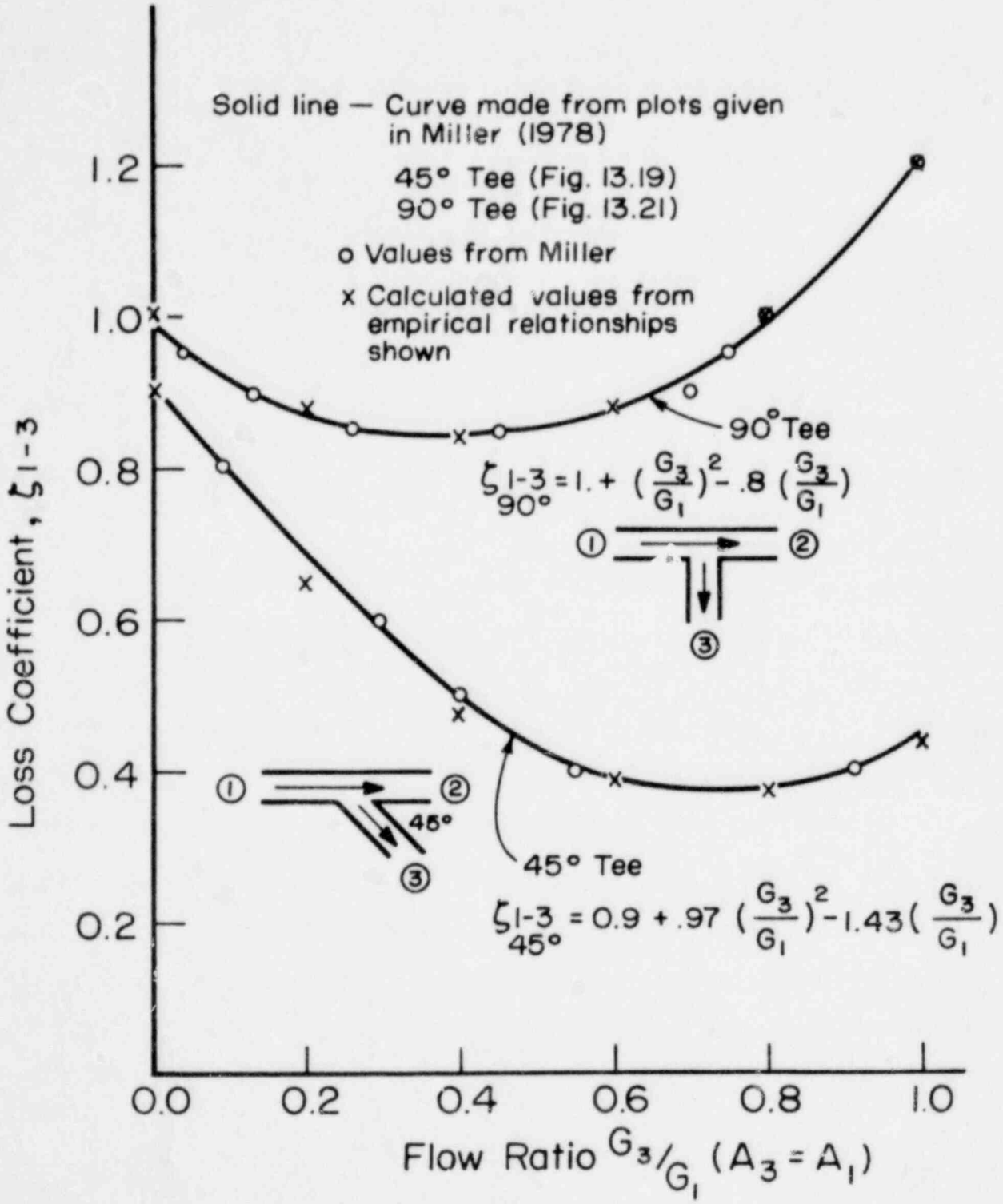

FIGURE II.5

Single-Phase Loss Coefficients in Wyes and Tees

$$\Delta p_{2J}-p_2 = \frac{1}{2g_c}\frac{G_2^2}{\rho_\ell} K_2 \phi_{\ell o_2}^2 + \bar{\rho}_2 \frac{g}{g_c} L_2 \qquad \text{(II.51)}$$

$$\Delta p_T = p_{1J}-p_{2J} = \zeta_{1-2}\left[\frac{G_2^2}{g_c<\rho_2^r>} - \frac{G_1^2}{g_c<\rho_1^i>}\right] \qquad \text{(II.52)}$$

where,

$$\frac{1}{<\rho_i^r>} \triangleq \left[\frac{(1-x_i)^2}{\rho_\ell (1-<\alpha_i>)} + \frac{x_i^2}{\rho_v <\alpha_i>}\right] \qquad \text{(II.53)}$$

ζ_{1-2} is a empirical pressure recovery factor, which is expected to be a function of G_2/G_1. In single-phase flow, the momentum correction factor, ζ_{1-2}, has been evaluated experimentally by Acrivos, et a. [12].

So far we have only stated four (4) independent conservation equations; the extra equation needed for closure of the problem is the vapor phase momentum equation. The vapor-phase momentum equation for the situation in which, $\rho_v << \rho_\ell$, is given by,

$$0 = -<\alpha>\nabla p + M_v \qquad \text{(II.54)}$$

Integrating along a "bubble" streamline through the branch we obtain,

$$\Delta p_{1-3} = \int_{J_1}^{3} \frac{-M_v}{<\alpha>} ds \qquad \text{(II.55)}$$

The reason for integrating along a streamline which enters into the side branch, rather than following one that continues in the straight run past the T-junction, is that the ability of a void to make the turn into the side branch is the dominant factor which affects the distribution of two-phase mixtures at a T-junction.

The volumetric momentum transfer term, M_v, for our case, is essentially the drag force on a bubble,

$$M_v = <\alpha> F_d = \frac{3<\alpha>}{4} \frac{\rho_\ell}{g_c} \frac{C_D}{D_b} u_r^2 \qquad \text{(II.56)}$$

Proceeding as before, the integral in equation (II.55) can be divided into three (3) segments, and can be approximated by the mean value theorem. Thus equation (II.55) becomes,

$$\Delta p_{1-3} = \int_{1}^{1J} \frac{-M_v}{\langle\alpha\rangle} ds + \int_{1J}^{3J} \frac{-M_v}{\langle\alpha\rangle} ds + \int_{3J}^{3} \frac{-M_v}{\langle\alpha\rangle} ds$$

or,

$$\Delta p_{1-3} = \frac{3}{4} \frac{\rho_\ell}{g_c} \left(\frac{C_D}{D_b}\right)_1 u_{r_1}^2 L_1 + \frac{3}{4} \frac{\rho_\ell}{g_c} \left(\frac{C_D}{D_b}\right)_J U_{r_J}^2 L_J + \frac{3}{4} \frac{\rho_\ell}{g_c} \left(\frac{C_D}{D_b}\right)_3 u_{r_3}^2 L_3 \quad \text{(II.57)}$$

where,

$\left(\frac{C_D}{D_b}\right)$ in the cross-sectionally averaged one-dimensional drag coefficient (having dimensions of reciprocal length). This coefficient is a function of $\langle\alpha\rangle$, the cross-sectionally averaged void fraction. For bubbly flows the following correlation was shown [5] to be valid,

$$(C_D/D_b) = 3.936 - 15.24\ (\langle\alpha\rangle), cm^{-1} \quad \text{(II.58)}$$

when,

$$0.125 \leq (\langle\alpha\rangle) \leq 0.22$$

For churn-turbulent flow, Hench, et al [13] used,

$$(C_D/D_b) = 0.549\ (1-\langle\alpha\rangle)^3, cm^{-1} \quad \text{(II.59)}$$

The length L_J in equation (II.57) can be viewed as an equivalent length which makes the total pressure change experienced by a bubble flowing along a streamline, from station-1 to station 3, equal to that of the mixture pressure drop. L_J is expected to be a function of inlet quality, x_1, and the flow-split ratio, G_3A_3/G_1A_1. Thus,

$$L_J = L_J\ (x_1,\ G_3A_3/G_1A_1) \quad \text{(II.60)}$$

Void fractions and relative velocities can be determined from standard drift-flux relationships. Following the analysis presented in [6], we have,

$$\langle\alpha\rangle = \frac{x}{C_o[x + \frac{\rho_v}{\rho_\ell}(1-x)] + \rho_v \frac{V_{gj}}{G}} \tag{II.61}$$

$$U_r \triangleq \langle u_v\rangle_v - \langle u_\ell\rangle_\ell$$

$$= \frac{\langle j\rangle (C_o-1) + V_{gj}}{(1-\langle\alpha\rangle)} \tag{II.62}$$

$$\langle j\rangle = G\left[\frac{x}{\rho_v} + \frac{1-x}{\rho_\ell}\right] \tag{II.63}$$

The concentration parameter, C_o, is defined as,

$$C_o \triangleq \langle j\alpha\rangle / \langle j\rangle\langle\alpha\rangle \tag{II.64}$$

This parameter has a value of about 1.1 for bubbly flow and 1.0 for homogeneous flow.

The drift-velocity, V_{gj}, is defined by,

$$V_{gj} \triangleq \langle\alpha(u_g - j)\rangle / \langle\alpha\rangle \tag{II.65}$$

For bubbly and churn-turbulent pipe flow we can use,

$$V_{gj} = 1.53\left[\frac{(\rho_\ell-\rho_v)}{\rho_\ell^2}\sigma g g_c\right]^{1/4} \sin\theta \tag{II.66}$$

We now have the required number of independent conservation equations, thus a solution scheme can be readily set up to solve for the unknown flow parameters. Unfortunately, we must have explicit information on $\zeta_{1-3}(\frac{A_3}{A_1}, G_3/G_1)$, $\zeta_{1-2}(G_2/G_1)$ and $L_J(x_1, G_3A_3/G_1A_1)$ before we can proceed. In order to deduce this information we need data on the pressure drops, Δp_{1-3} and Δp_{1-2}, to supplement the measured phase separation results [9]. It is planned to take such data in the near future.

TASK III

BWR ECC PARALLEL CHANNEL EFFECTS

There are numerous cases of safety significance in light water nuclear reactors (LWR) in which a knowledge of parallel channel interactions during counter-current flow limited (CCFL), ie: flooding, conditions are important. Examples include questions of PWR upper head injection (UHI) system performance and BWR top spray system performance.

The specific problem which is being addressed under this task is concerned with the parallel channel effects (PCE) which may occur during the top spray (ECCS) phase of a hypothetical BWR LOCA event.

III.1 PCE Experimental Facility

A large experimental facility, which will employ Freon-114 to study the possibility of BWR "vapor-binding", is under construction.

During the Eleventh Quarter, the following significant items were accomplished on the PCE loop:

- A leaking gasket on the R-22 condenser bonnet was discovered and replaced.
- While the R-22 system was down, the pressure and differential pressure transducers were installed and checked-out.
- The R-114 transfer loop was evacuated and charged with Freon.
- Freon was circulated through the transfer loop to clean the pipes.
- The relief valve problem reported in the Tenth Quarterly report [5] was solved as follows:
  - The leaky 50 PSIG valves on the heater vessels were replaced by in-line refrigeration valves set at 150 PSIG.

- In order to protect the glass test section, the test section and storage tank will be protected by rupture disks with 50 PSIG burst ratings. The rupture disks can be replaced by closing valves on the discharge of the test section and storage tank. These valves will be locked open except as required during maintenance.
- By the end of the Eleventh Quarter only one relief valve had not yet been received.

- The five calibrated 1/4" orifice assemblies for measuring test section flow rates were received and installed.
- The process instrumentation(thermocouples, absolute and differential pressure transducers) were installed and wired up.
- The system was modified by adding drain lines from the heater vessels to the suction side of the transfer pump.
- The parallel channel expansion joints were fabricated
- The test section glassware was assembled for proof testing with:
  - Dummy rods used in place of instrumented heater rods.
  - Electrical and signal feed-throughs installed and connected.
  - Differential pressure transducers connected to the parallel channels.
  - Lower plenum sight windows installed.
- The test section was leak checked. During evacuation, several poor welds were discovered in the lower half of the upper plenum. These were sealed temporarily (with putty) to allow leak checking. No detectable leaks were discovered at the glass pipe flanges, glass pipe pressure taps, or "o" ring seals. By the end of the report period, work was underway to repair the defective welds.

III.2 PCE Data Aquisition System

A new executive system (DOS-15 V3A) was brought up on the PDP-9 computer. This greatly increased our computer power but required extensive rewriting of the data aquision and reduction software. By the end of the report period this work was well underway. It appears, however, that, even with this new system, our data transfer rate will be limited, thus we are currently looking at methods to improve data aquisition during the "burst" mode of aquisition.

By the end of the Eleventh Quarter the low level multiplexer boards had been built and were being checked out (assembly of the high level boards is planned for the next quarter). During this check out it was discovered that the CAMAC A/D converter did not contain the L.P. filters which were ordered (10Hz break frequency). Thus this system was returned to the factory to rectify this situation.

III.3 PCE Analysis

In accordance with our agreement with Dr. S. Fabic, a scaled water version of the actual Freon-114 BWR parallel channel effects (PCE) experiment at RPI has been modelled on TRAC and a deck submitted to LASL. Since TRAC now has only water properties, we have had to scale our Freon experiment to equivalent water condition. In the near future, we will be developing Freon property routines which are compatible with TRAC. When these are available, we plan to simulate(with TRAC)the actual Freon test matrix we will be testing. Until then, the equivalent water case should give us valuable insight into our experiment and TRAC's ability to predict it.

The test case submitted is to study the potential for steam binding during a postulated loss-of-coolant-accident (LOCA) in a BWR. A schematic of the RPI PCE loop is shown in figure III.1. The equivalent TRAC schematic is shown in figure III.2.

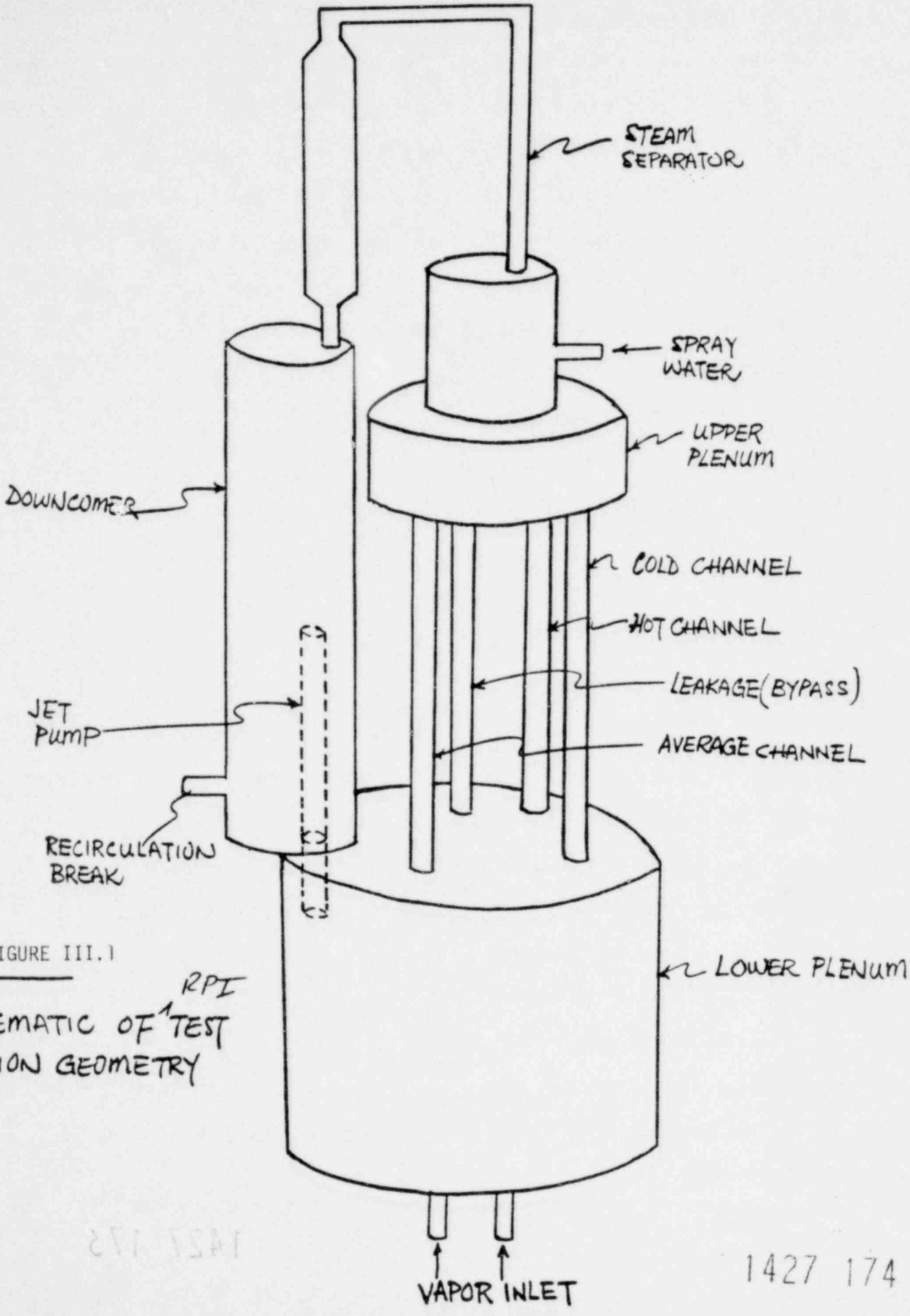

FIGURE III.1

SCHEMATIC OF TEST SECTION GEOMETRY RPI

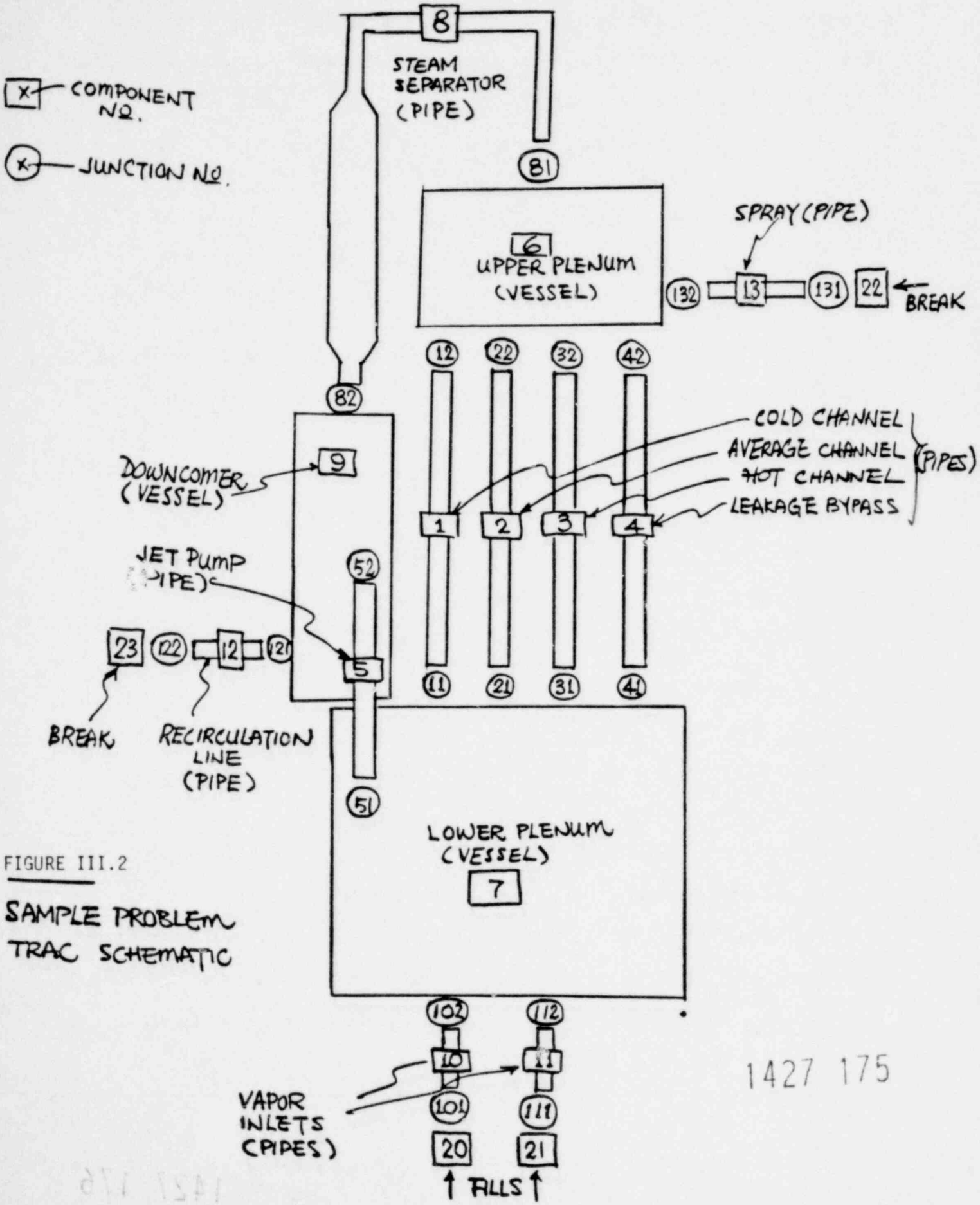

FIGURE III.2

SAMPLE PROBLEM TRAC SCHEMATIC

The lower plenum, upper plenum and downcomer region are modeled using three vessels. The dimensions and noding are shown in figures III.3, III.4 and III.5, respectively. The steam separator is simulated by an unheated pipe, and is shown in figure II.6.

The average heat fluxes*(uniform axial heat flux profiles on all rods) in the heated channels are,

- Cold channel: 5,020 BTU/ft^2-hr
- Average channel: 7,525 BTU/ft^2-hr
- Hot channel: 10,075 BTU/ft^2-hr

An additional unheated tube is used to simulate the leakage (ie: bypass) flow path from plenum-to-plenum in the BWR. The dimensions and noding for the channels are shown in figure III.7.

Initially, the lower plenum is partially filled with saturated water, while the rest of the system is assumed filled with saturated steam at 200 psia. Saturated steam is injected into the bottom of the lower plenum to simulate the vapor produced by vessel heat transfer.

The assumed initial conditions are:

- system pressure = 200 psia
- system temperature = 382°F
- water level = 1.736 m. in. the lower plenum
- spray water rate = 0.0 gpm
- total vapor inlet rate (saturated at 200 psia) = 16,800 lb_m/hr
- jet pump recirculation line break pressure = 1 atmosphere

At the beginning of the transient calculation, subcooled water at 100°F is introduced into the upper plenum at a constant rate of 54.8 gpm. The inlet vapor flow rate is held at 16,800 lb_m/hr for 0.5 minutes and then is allowed to

---

*decay heat levels

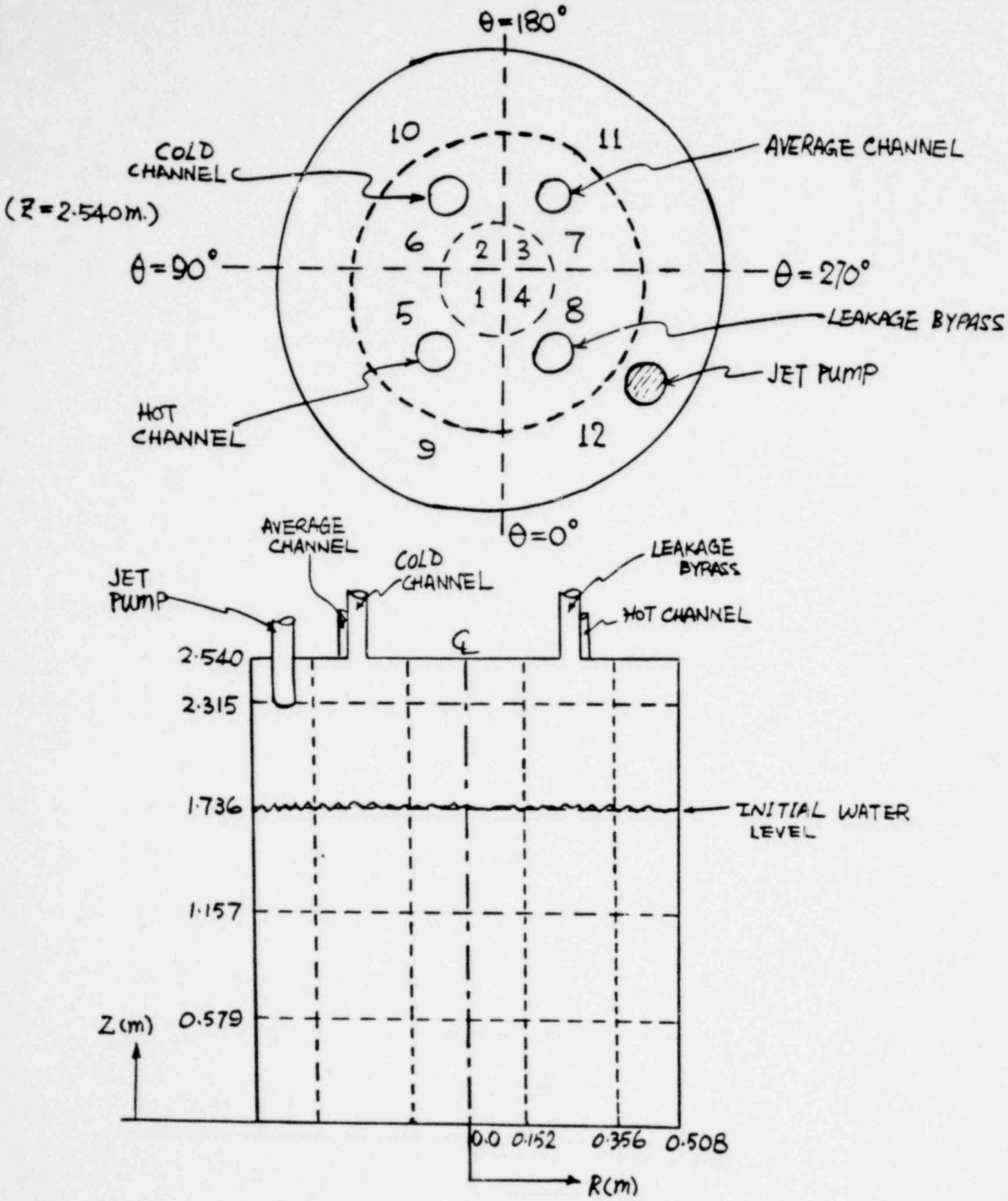

FIGURE III.3 TRAC NODING FOR LOWER PLENUM

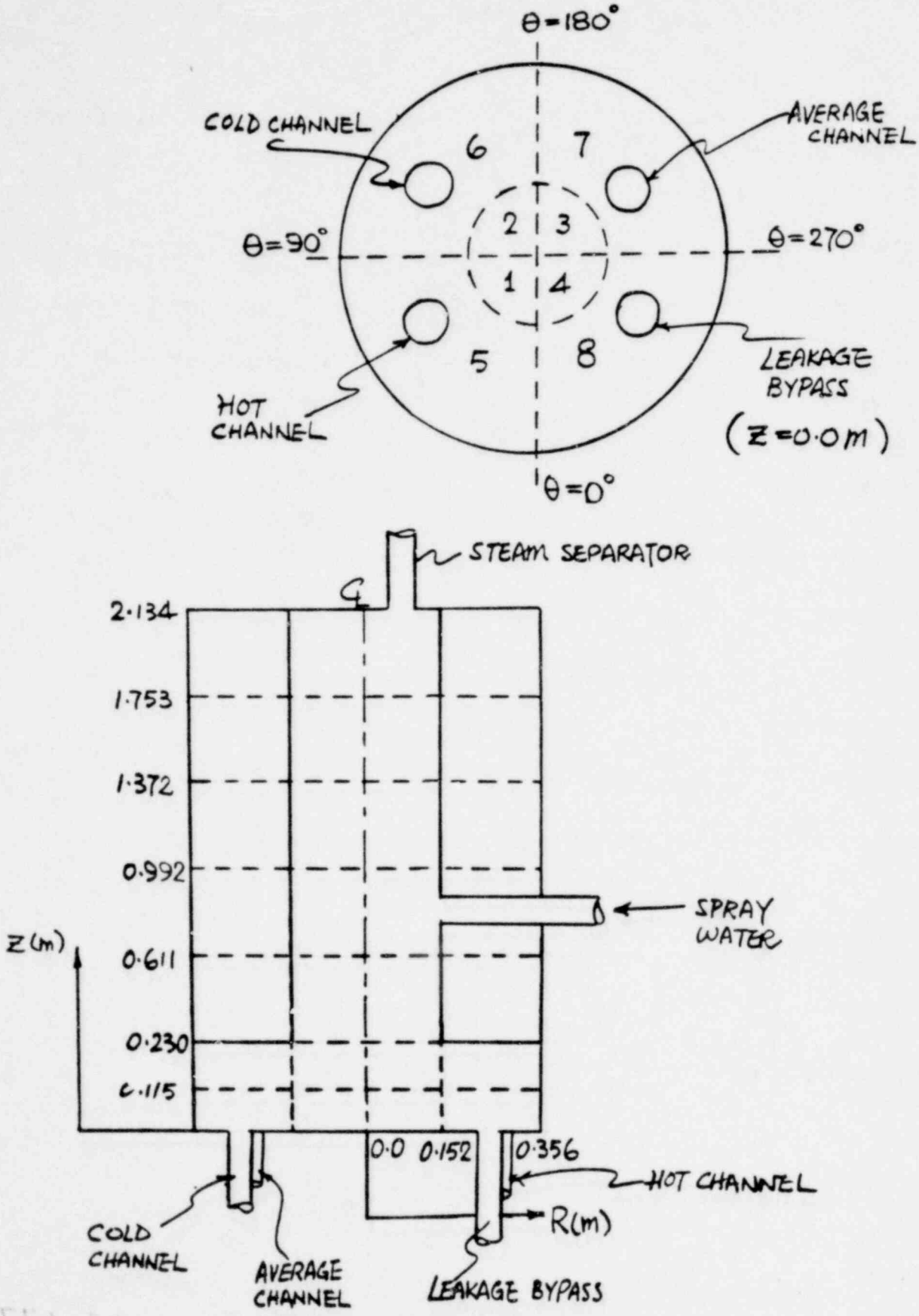

FIGURE II.4 TRAC NODING FOR UPPER PLENUM

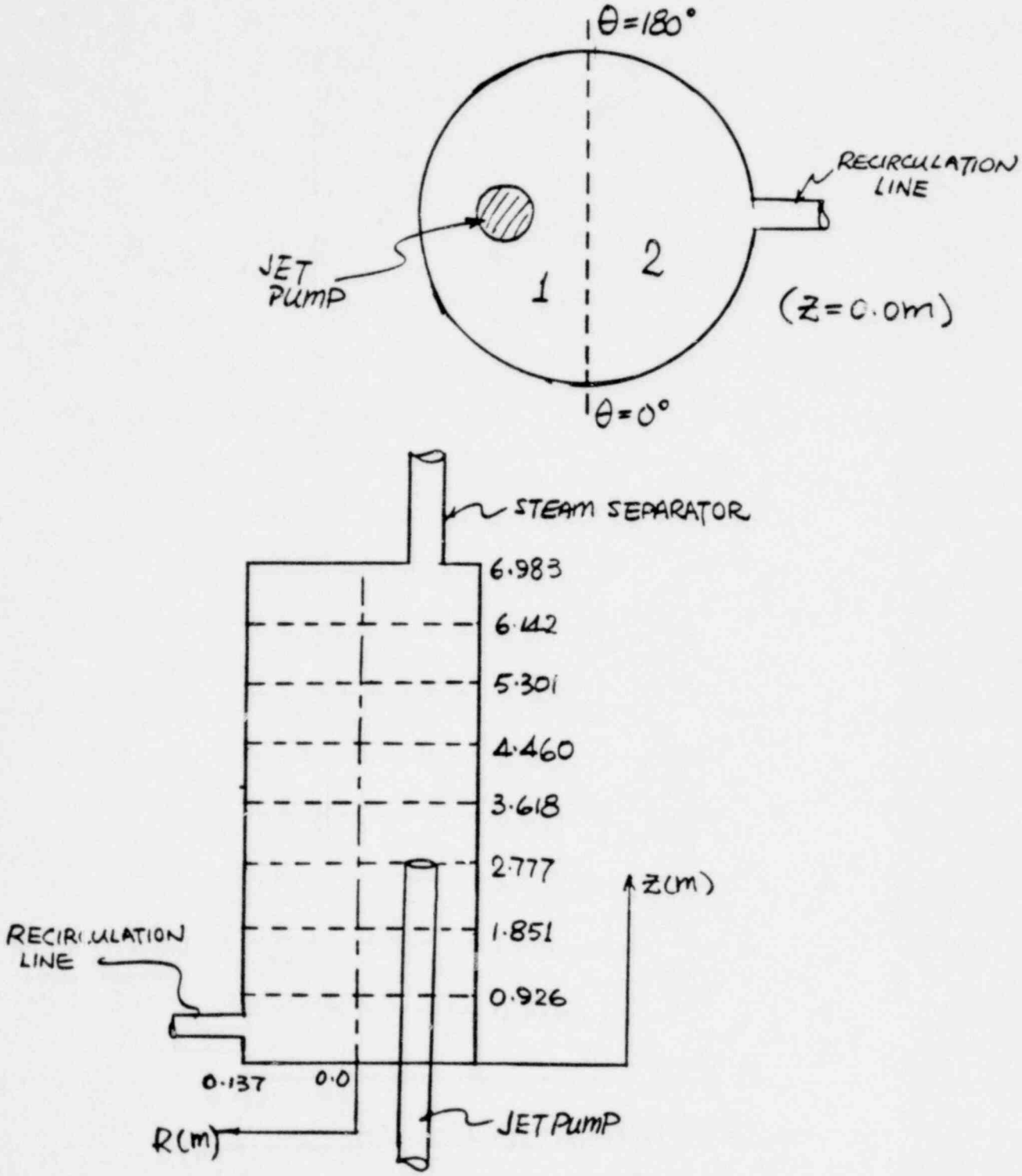

FIGURE III.5 TRAC NODING FOR DOWNCOMER

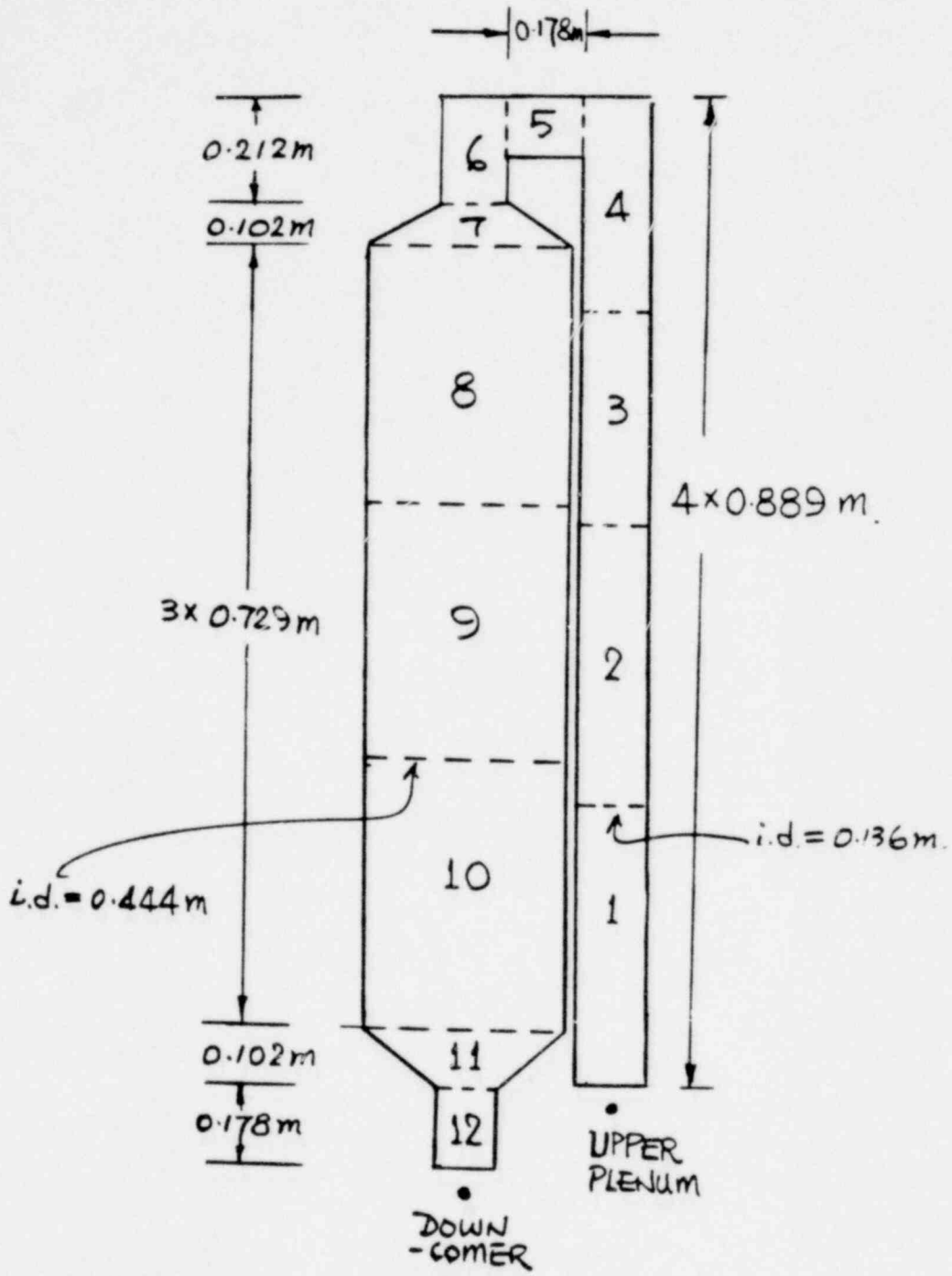

FIGURE III.6 TRAC NODING FOR STEAM SEPARATOR

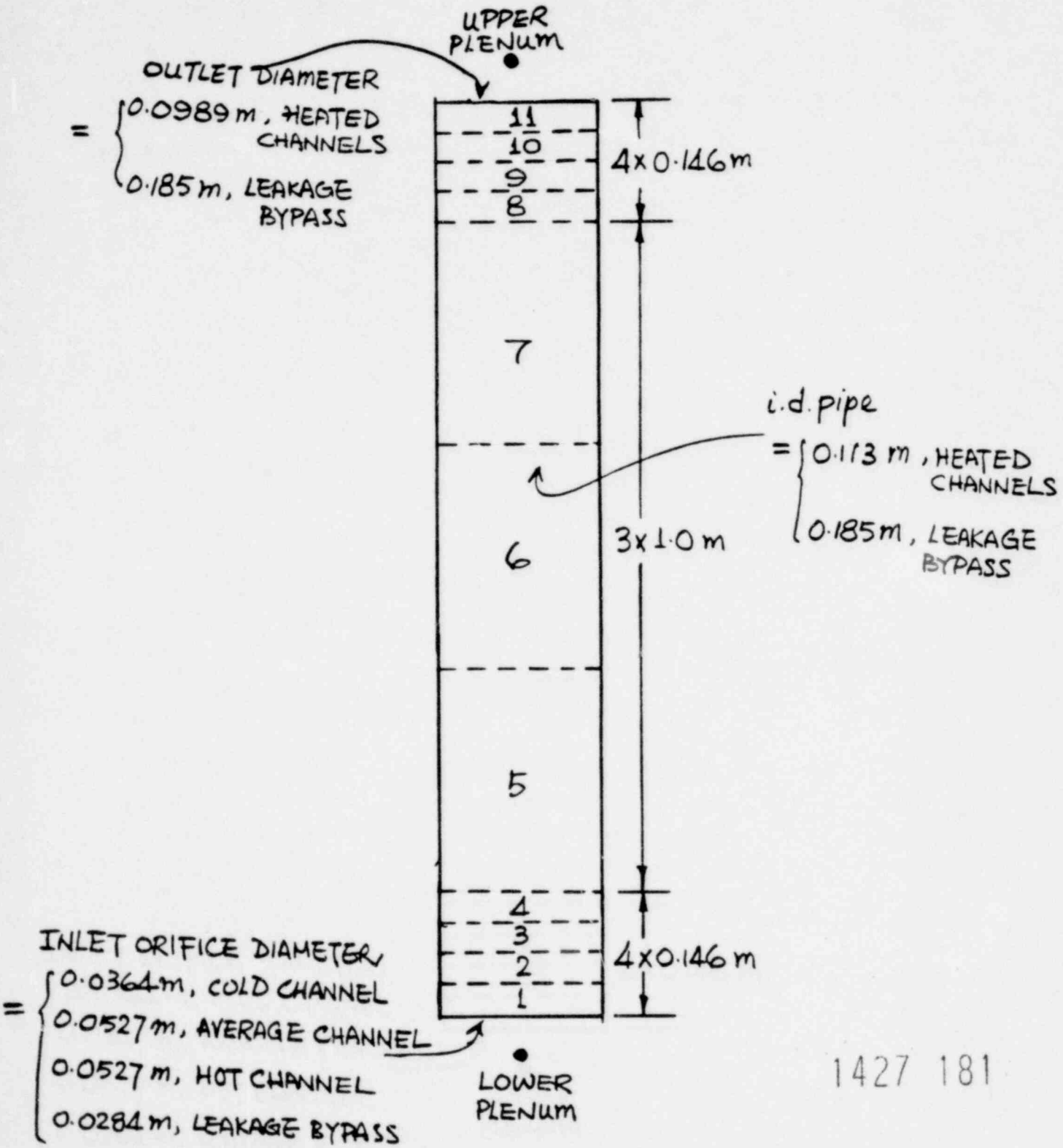

1427 181

FIGURE III.7 TRAC NODING FOR THE HEATED CHANNELS AND LEAKAGE BYPASS

decay exponentially to 140 lb_m/hr in a time interval of 1.5 minutes. A total transient calculation time of 5.0 minutes was specified in the deck submitted to LASL.

While remote calculations leave a lot to be desired, it is felt that LASL will be able to give us reasonable service on this and subsequent runs.

ACKNOWLEDGEMENTS

The advice and assistance of the following individuals, given to the program during the Eleventh Quarter, is gratefully acknowledged.

- Professor Rodney Gay (RPI)
- Professor Robert C. Block (RPI)
- Mr. Ernie Muzzey (RPI)

TECHNICAL PAPERS AND REPORTS RESULTING FROM RESEARCH PROGRAM

Topical Reports

(1) Cheng, L.Y., Drew, D.A., Lahey, R.T. Jr., "Virtual Mass Effects in Two-Phase Flow", NUREG/CR-0020, 1978.

(2) Honan, T. and Lahey, R.T., Jr., "The Measurement of Phase Separation in Wyes and Tees", NUREG/CR-0557, 1978.

(3) Schell, Susanne, L., Gay, R.R., Lahey, R.T., Jr., "The Development of a Side-Scatter Gamma Ray System for the Measurement of Local Void Fraction", NUREG/CR-0677, 1978.

R.P.I. Thesis (Not Published As Topical Reports)

(1) Saba, N., "An Experimental Technique for the Determination of Steam/Air Fraction", M.S. thesis, November, 1977.

(2) Sim, S.K., "Analysis of Phase Distribution Mechanisms in Turbulent Two-Phase Pipe Flow", M.S. thesis, December, 1977.

(3) Shum, F.B., "The Development of a Four Equation Drift-Flux Computer Code (DRIFT-4)", M.S. thesis, May, 1978.

(4) Lombardo, N.J., "The Development of a Data Acquisition and Reduction System for the RPI BWR Parallel Channel Effects Experiment", M.E. thesis, December, 1978.

Technical Papers

(1) Saba, N., Krycuk, G. and Lahey, R.T., Jr., "An Experimental Technique for the Determination of Steam/Air Fraction", ANS Transactions, Vol.-27, 1977.

(2) Block, R.C., Perez-Griffo, M., Singh, U.N., and Lahey, R.T., Jr., "N^{16} Tagging of Water for Transient Flow Measurements", ANS Transactions, Vol.-27, 1977.

(3) Perez-Griffo, M., Block, R.C. and Lahey, R.T., Jr., "N^{16} Tagging for Two-Phase Flow Measurements", ANS Transactions, Vol.-30, 1978.

(4) Lahey, R.T., Jr., Krycuk, G. and Malaviya, B.K., "A High Intensity X-ray System for Stochastic Measurements of Two-Phase Flows", ANS Transactions, Vol-30, 1978.

(5) Vince, M., Breed, H.E. and Lahey, R.T., Jr., "The Development of a High Temperature Optical Void Probe", ANS Transactions, Vol.-30, 1978.

(6) Gay, R.R., Schell, S. and Lahey, R.T., Jr., "The Side-Scatter Gamma Technique for Local Density Measurements", ANS Transactions, Vol.-30, 1978.

(7) Moreira, S. Krycuk, G. and Lahey, R.T.,Jr., "Development of a Radio-Frequency Local Probe for Void Fraction Measurements", ANS Transactions, Vol.-30, 1978.

(8) Lahey, R.T.,Jr., Cheng, L.Y., Drew, D.A. and Flaherty, J.E., AIChE paper #56b, presented at 71st AIChE Meeting, Miami, 1978.

(9) Drew, D.A., Sim, S. and Lahey, R.T., Jr., "Radial Phase Distribution Mechanisms in Two-Phase Flow", Proceedings of the CSNI Specialists Meeting on Transient Two-Phase Flow, Paris, 1977.

(10) Lahey, R.T., Jr., Vince, M. and Krycuk, G., "The Development of an Optical Digital Interferometer", Proceedings of the 2nd Multi-Phase Flow and Heat Transfer Symposium Workshop, April, 1979, Miami, Florida.

(11) Lahey, R.T., Jr., and Drew, D.A., "The Analysis of Phase Distribution in Fully Developed Two-Phase Flows", Proceedings of the 2nd Multi-Phase Flow and Heat Transfer Symposium Workshop, April, 1979, Miami, Florida.

(12) Honan, T.J., and Lahey, R.T., Jr., "The Analysis of Dynamic Bias in Gamma Densitometer Measurements", ANS Transactions, Vol.-32, 1979.

(13) Honan, T.J. and Lahey, R.T., Jr., "The Evaluation of Static Error in Gamma Densitometry", ANS Transactions, Vol.-32, 1979.

(14) Conlon, W.M. and Lahey, R.T., Jr., "Scaling of the RPI Parallel Channel Effects Experiment", ANS Transactions, Vol.-32, 1979.

(15) Gay, R.R. and Lahey, R.T.,Jr., "Dynamic Bias in Side-Scatter Gamma Density Measurements", ANS Transactions, Vol.-32, 1979.

(16) Lahey, R.T., Jr., Sim, S. and Drew, D.A., "An Evaluation of Interfacial Drag Models for Bubbly Two-Phase Flows", ASME Symposium Volume on, Interfacial Transport Phenomena, 1979 National Heat Transfer Conference, San Diego, California, 1979.

REFERENCES

[1] Lahey, R.T., Jr., QUARTERLY PROGRESS REPORT #6, September 1, 1977-November 31, 1977, "Two-Phase Flow Phenomena in Nuclear Reactor Technology", 1977.

[2] Taylor, G.I., Proc. Roy. Soc. London, Ser. A219 and 223, 1953.

[3] Lahey, R.T., Jr., QUARTERLY PROGRESS REPORT #8, March 1, 1978 - May 31, 1978, "Two-Phase Flow Phenomena in Nuclear Reactor Technology," 1978.

[4] Serizawa, A., Kataoka, I. and Michiyoshii , I., "Turbulent Structure of Air/Water Bubble Flow", Int. J. Multiphase Flow, 2, 1975.

[5] Lahey, R.T., Jr., QUARTERLY PROGRESS REPORT #10, "Two-Phase Flow Phenomena in Nuclear Reactor Technology", September 1, 1978 - November 30, 1978.

[6] Lahey, R.T.,Jr., and Moody, F.J., "The Thermal-Hydraulics of a Boiling Water Nuclear Reactor", ANS Monograph, 1977.

[7] Lahey, R.T., Jr., QUARTERLY PROGRESS REPORT #9, "Two-Phase Flow Phenomena in Nuclear Reactor Technology", June 1, 1978 - August 31, 1978.

[8] Zienkiewicz, O.C., "The Finite Element Method" Third Edition, McGraw-Hill, London, 1977.

[9] Honan, T.J. and Lahey, R.T., Jr., "The Measurement of Phase Separation in Wyes and Tees", NUREG/CR-0557, 1978.

[10] Chisholm, D., "Pressure Losses in Bends and Tees During Steam-Water Flow", NEL Report #318, 1967.

[11] Miller, D.S., "Internal Flow Systems", BHRA Fluid Engineering, 1978.

[12] Acrivos, A., Bacock, B.D. and Pigford, R.L., "Flow Distribution in Manifolds", Chem. Eng. Sci., 10, 1959.

[13] Hench, J.E. and Johnston, J.P., "Two-Dimensional Diffuser Performance with Subsonic Two-Phase Air/Water Flow", APED-5477, 1968.

RPI Folsom Library (H. Spence)
*RPI Departmental Library
USNRC Contract Officer - (2)
A. W. Savolainen (USNRC)
**Dr. S. Fabic (USNRC)
*Dr. Y. Y. Hsu (USNRC)
Dr. Z. Rosztoczy (USNRC)
**Dr. L. S. Tong (USNRC)
*Dr. N. Zuber (USNRC)
Dr. D. Groeneveld (AECL)
Dr. R. Henry (ANL)
**Dr. M. Ishii (ANL)
Dr. P. Kehler (ANL)
Dr. P. A. Lottes (ANL)
Dr. W. T. Sha (ANL)
Dr. O. C. Jones (BNL)
*Dr. J. M. Delhaye (CEA)
**Dr. T. Fernandez (EPRI)
Dr. G. E. Dix (GE)
Mr. Keith Condie (INEL)
Dr. P. Jallouk (ORNL)
Professor S. G. Bankoff (Northwestern)
**Professor G. Birkoff (Harvard)
Professor G. Carrier (Harvard)
**Dr. J. Chen (Lehigh)
Dr. S. C. Cheng (U of Ottawa)
**Dean A. Dukler (U of Houston)
**Professor P. G. Griffith (MIT)
Professor P. Lax (NYU)
Dr. R. Lee (SUNY/Stonybrook)
Professor F. Marble (Cal. Tech.)
**Professor K. Miller (UC-Berkeley)
Professor V. Schrock (UC-Berkeley)
Professor C. Truesdell (Johns Hopkins)
Dr. G.B. Wallis/Dr. H. Richter (Dartmouth)
*Professor H. E. Breed (RPI)
*Professor D. A. Drew (RPI)
*Professor J. E. Flaherty (RPI)
*Professor R. R. Gay (RPI)
*Professor R. C. Block (RPI)
*Mr. G. Krycuk (RPI)
*Professor R. T. Lahey, Jr. (RPI)
*Mr. J. Tully (RPI)
*Mr. M. Barasch (RPI)
*Mr. K. Ohkawa (RPI)
*Mr. L. Cheng (RPI)
*Mr. W. Conlon (RPI)
*Mr. M. Fakory (RPI)
*Mr. S. Moreira (RPI)
*Mr. N. Saba (RPI)
*Mr. D. Shum (RPI)
*Mr. S. Sim (RPI)
*Mr. M. Vince (RPI)
Professor J. M. Gonzalez-Santalo (Mexico)
Professor S. Banerjee (McMasters)
Professor J. Bataille (Lyon)
Mr. G. L. Shires (AEE/Winfrith)
Dr. S. H. Chan (U. of Wisconsin/Milwaukee)
M. H. Fontana (ORNL)
Dr. J. L. Achard (RPI)
Dr. L. Wolf (BNL-F)

*Receive preliminary copy prior to NUREG report
**On standard NUREG distribution list

NRC FORM 335 (7-77) U.S. NUCLEAR REGULATORY COMMISSION

BIBLIOGRAPHIC DATA SHEET

1. REPORT NUMBER (Assigned by DDC): NUREG/CR-1130

4. TITLE AND SUBTITLE (Add Volume No., if appropriate)
Two-Phase Flow Phenomena in Nuclear Reactor Technology
Quartely Progress Report No. 11
December 1, 1978 - February 28, 1979

2. (Leave blank)

3. RECIPIENT'S ACCESSION NO.

7. AUTHOR(S)
R. T. Lahey, Jr.

5. DATE REPORT COMPLETED
MONTH: April YEAR: 1979

9. PERFORMING ORGANIZATION NAME AND MAILING ADDRESS (Include Zip Code)
Department of Nuclear Engineering
Rensselaer Polytechie Institute
Troy, New York 12181

DATE REPORT ISSUED
MONTH: October YEAR: 79

6. (Leave blank)

8. (Leave blank)

12. SPONSORING ORGANIZATION NAME AND MAILING ADDRESS (Include Zip Code)
Separate Effects Branch
Division of Reactor Safety Research
U. S. Nuclear Regulatory Commission
Washington, DC 20555

10. PROJECT/TASK/WORK UNIT NO.

11. CONTRACT NO.
NRC-04-76-301

13. TYPE OF REPORT
Research Project Progress Report

PERIOD COVERED (Inclusive dates)
December 1, 1978 - February 28, 1979

15. SUPPLEMENTARY NOTES

14. (Leave blank)

16. ABSTRACT (200 words or less)

This Quarterly Progress Report contains a description of the work done in three areas of technology. The significant results are:

I. Two-Phase Flow Instrumentation Development - The recent PNA tagging data is presented. In addition, a detailed error analysis is presented for the side-scatter gamma ray system under development.

II. Phase Distribution and Separation Phenomena - An analytical model for phase separation in Wyes and Tees is presented. In addition, an analytical model for subchannel void-drift is developed.

III. BWR Parallel Channel Effects - The status of the experimental PCE loop and the supporting analysis is presented.

17. KEY WORDS AND DOCUMENT ANALYSIS

17a. DESCRIPTORS

1427 189

17b. IDENTIFIERS/OPEN-ENDED TERMS

18. AVAILABILITY STATEMENT
Unlimited

19. SECURITY CLASS (This report): Unclassified

21. NO. OF PAGES

20. SECURITY CLASS (This page)

22. PRICE
$

NRC FORM 335 (7-77)

POOR ORIGINAL